Propagation of a sudden impulse through the magnetosphere initiating magnetospheric Pc5 pulsations

A. A. Samsonov,[1,2] D. G. Sibeck,[3] N. V. Zolotova,[2] H. K. Biernat,[1] S.-H. Chen,[3] L. Rastaetter,[3] H. J. Singer,[4] and W. Baumjohann[1]

Received 31 March 2011; revised 13 July 2011; accepted 22 July 2011; published 18 October 2011.

[1] We compare multipoint observations of an interplanetary shock's interaction with the Earth's magnetosphere on 29 July 2002 with results from global MHD simulations. The sudden impulse associated with the shock's arrival initiates global ultralow-frequency waves with periods from 2 to 5 min. We interpret four cycles of Bz oscillations with T = ~3 min at Geotail in the postdawn magnetosphere as radial magnetopause oscillations. GOES 8, in the same late morning sector, observed compressional and toroidal waves with the same frequency at the same time. GOES 10, in the early morning sector, observed toroidal waves with a slightly lower period. We suggest that these observations confirm the mode coupling theory. The interplanetary shock initiates compressional magnetospheric waves which, according to our estimates, oscillate between the ionosphere and magnetopause and gradually convert their energy into that of standing Alfven waves. At the same time, Polar in the outer predawn magnetosphere observed strong velocity oscillations and weak magnetic field oscillations with a ~4 min period. Global MHD models successfully predict these oscillations and connect them to the Kelvin-Helmholtz instability which results in large flow vortices with sizes of about ten Earth radii. However, the global models do not predict the multiple compressional oscillations with the observed periods and therefore cannot readily explain the GOES observations.

Citation: Samsonov, A. A., D. G. Sibeck, N. V. Zolotova, H. K. Biernat, S.-H. Chen, L. Rastaetter, H. J. Singer, and W. Baumjohann (2011), Propagation of a sudden impulse through the magnetosphere initiating magnetospheric Pc5 pulsations, *J. Geophys. Res.*, *116*, A10216, doi:10.1029/2011JA016706.

1. Introduction

[2] Interplanetary shocks (IS) associated with strong and sharp increases in the solar wind dynamic pressure compress the Earth's magnetosphere and intensify the magnetospheric-ionospheric currents [*Samsonov et al.*, 2010, and references therein]. In ground-based magnetometer data, sudden impulse variations are observed at the shock arrival time. The sudden impulse is registered as an increase of the horizontal (H) magnetic field component that occurs almost simultaneously at low and midlatitude stations, whereas magnetic field variations at high-latitude stations consist of preliminary and main impulses [*Araki*, 1994]. The arrival of an IS sometimes coincides with the onset of a magnetic storm or substorm [*Zhou and Tsurutani*, 2001] depending on the IMF (interplanetary magnetic field) conditions. The magnetospheric response can be different for shocks aligned with the Sun-Earth line and for strongly inclined shocks [*Samsonov*, 2011]. We confine our attention here to the shocks with normals nearly along the Sun-Earth line which are more frequently observed.

[3] Let us summarize the relevant aspects concerning shock interaction with the magnetosphere, as gathered from the last fifty years. IS are usually described by magnetohydrodynamic (MHD) theory as forward fast shocks whose jump conditions obey the Rankine-Hugoniot relations. The interaction of a such shock with the bow shock results in different combinations of discontinuities [*Dryer*, 1973; *Grib*, 1982; *Pushkar et al.*, 1991; *Samsonov et al.*, 2006; *Grib and Pushkar*, 2010; *Samsonov*, 2011], but these combinations usually include a transmitted forward fast shock, a contact discontinuity with a density increase, and a reversed fast shock. The last is the bow shock with modified jump parameters moving Earthward in the Earth-centered frame. In the next step, the forward fast shock interacts with the magnetopause, which is assumed to be a tangential discontinuity. According to MHD predictions for the subsolar region, a forward fast shock having a fast Mach number, slightly more than unity, propagates through the magnetosphere, the magnetopause moves Earthward, and a fast rarefaction wave reflects back into the magnetosheath after the interaction [*Grib et al.*, 1979]. Although several new waves and discontinuities traverse the magnetosheath after the shock

[1]Space Research Institute, Graz, Austria.
[2]Saint Petersburg State University, St. Petersburg, Russia.
[3]NASA Goddard Space Flight Center, Greenbelt, Maryland, USA.
[4]Space Weather Prediction Center, NOAA, Boulder, Colorado, USA.

Copyright 2011 by the American Geophysical Union.
0148-0227/11/2011JA016706

passage, the fast shock going through the magnetosphere carries away most of the energy associated with the initial IS [*Samsonov et al.*, 2007].

[4] We will define the disturbance propagating through the magnetosphere and related to IS a sudden impulse (SI), since this term has been widely used in previous papers. The problem of SI propagation in the magnetosphere is difficult because the fast magnetosonic velocity is inhomogeneous, and the magnetospheric SI can be described as a superposition of waves from multiple sources along the magnetopause and reflected waves from the plasmapause or ionosphere. On the other hand, magnetospheric dynamics can be described in terms of electric current systems and magnetospheric magnetic fields can be calculated by summing the fields induced by all current systems and the Earth's dipole. Surely both methods, i.e., using the analysis of propagating MHD waves and the superposition of magnetic fields generated by the electric currents, should give the same result.

[5] *Dessler* [1958] and *Francis et al.* [1959] first explained SI propagation through the magnetosphere in terms of hydromagnetic waves. *Francis et al.* [1959] calculated the transit time from the subsolar magnetopause to the Earth using Fermat's principle. They assumed that the SI propagates with the Alfvén speed, but the magnetospheric ion density profile needed to calculate this velocity was unknown at the time. Following this approach, *Dessler et al.* [1960] explained why ground observations indicate SI risetimes of several minutes, i.e., an order of magnitude larger than the duration of IS in the solar wind. *Wilson and Sugiura* [1961] speculated that IS generate both longitudinal compressional waves in the low-latitude magnetosphere and transverse (Alfvén) waves propagating along field lines to the high-latitude ionosphere. The latter was assumed to explain the two-pulses structure commonly constituting SI in high latitudes. *Wilson and Sugiura* [1961] also noted that ground magnetic field oscillations with periods from 2.5 to 10 min often follow SIs. These SI oscillations occur preferentially at high rather than low-latitude stations. *Saito and Matsushita* [1967] proposed classifying the pulsations according to their periods in a manner similar to that for continuous pulsations (Pc), but naming the pulsations related to SI as Psc. Pulsations with longest periods in their classification (Psc 5 with T = 150–600 s) are observed in the auroral zone most frequently during the local morning hours.

[6] *Tamao* [1964] mathematically showed that sudden impulses excite converted Alfvén waves in the magnetosphere. *Chen and Hasegawa* [1974] and *Southwood* [1974] developed the theoretical background that explains field line resonances (i.e., standing Alfvén waves in the magnetosphere) which feeds on energy whether from the Kelvin-Helmholtz instability or from a sudden impulse propagating through the magnetosphere. *Hasegawa et al.* [1983] showed that field lines oscillate at their Alfven resonance frequency in response to a wide band source, like a SI, whose frequency range covers the resonance frequencies. According to *Kivelson and Southwood* [1985], the discrete spectra of the field line resonances are explained by resonant eigenfrequencies of fast mode waves in the outer magnetosphere. These cavity mode waves oscillate between inner turning points at large density gradients (e.g., the plasmapause) and the magnetopause [*Kivelson et al.*, 1984] or between the turning point and the bow shock [*Harrold and Samson*, 1992]. Later the waveguide model [*Samson et al.*, 1992; *Walker et al.*, 1992] took into account the fact that the waves can freely propagate in the tailward direction oscillating between the two boundaries.

[7] Coupling of the global compressional and toroidal standing waves was numerically simulated by *Lee and Lysak* [1989, 1991]. Recently *Claudepierre et al.* [2010] simulated ultralow-frequency (ULF) waves in the dayside magnetosphere driven by solar wind dynamic pressure variations using the global Lyon-Fedder-Mobarry (LFM) code. They imposed artificial monochromatic oscillations of the solar wind density with frequencies of 10, 15, and 25 mHz during a 5 h interval. Furthermore they made a fourth run with a quasi-continuous spectrum of frequencies. They found toroidal modes in the magnetosphere on field lines whose resonant frequencies correspond to the frequency of the input signal. This result also agrees with the coupling theory discussed above.

[8] In observations, *Baumjohann et al.* [1983, 1984] found damped compressional waves with periods of 2–4 min excited by a SI at the dayside geosynchronous orbit. *Baumjohann et al.* [1984] also reported on standing transverse Alfven waves observed simultaneously by the same spacecraft. In the statistical study, *Hudson et al.* [2004] found both compressional and transverse Pc5 oscillations in about half of events following SIs at geosynchronous orbit. There were also a few examples of purely compressional and purely toroidal waves.

[9] Although magnetospheric observations generally do not contradict the theoretical scenario outlined above, some important questions still need to be addressed. In our opinion, the boundaries for the oscillation region of compressional waves need not be the plasmapause and magnetopause. For example, *Shinbori et al.* [2004] observed damped electric and magnetic field oscillations well inside the plasmasphere (L = 2.5) near the equatorial plane with periods in the Pc 3–4 range (40–150 s) after SIs. As shown with the three-dimensional solution of linearized wave equations in the dipole magnetic field configuration by *Lee and Hudson* [2001], sudden impulses penetrate very deep into the plasmasphere reaching the inner numerical boundary at L = 2 and excite transverse waves predicted in the polar region even on small L shells. According to *Lee and Hudson* [2001], waves oscillate throughout the entire region between inner and outer numerical boundaries (the outer boundary in their model is the fixed magnetopause). *Samsonov et al.* [2007] used a simple one-dimensional MHD model at the Sun-Earth line to show that most SI energy penetrates into the plasmasphere and only about 30 percent reflects back from the plasmapause into the outer magnetosphere.

[10] The three-dimensional MHD simulation with the BATS-R-US magnetospheric code used by *Samsonov et al.* [2007] showed that the SI reflects from the inner numerical boundary as a reflected fast shock (or a fast wave). The reflected shock moves sunward, passes through the magnetopause and interacts with the bow shock. This interaction results in a sunward bow shock motion, and another earthward propagating discontinuity (or MHD wave) reflects into the magnetosheath. *Pallocchia et al.* [2010] obtained the same numerical result simulating one real event of an interplanetary shock–magnetosphere interaction with the 3-D MHD local magnetosheath model. The simulation shows that the new discontinuity is characterized by a decrease of density

and magnetic field magnitude, and an increase of temperature. In fact, Cluster observes a similar discontinuity, but in the observations the decrease in density and increase in temperature coincides with increase in magnetic field. The observations from four Cluster spacecraft allow making the conclusion that this discontinuity propagates with the local plasma speed and has a minuscule normal magnetic field component, therefore resembling a tangential discontinuity.

[11] In addition to this magnetosheath discontinuity, the interaction between the reflected fast shock and the magnetopause in the global MHD simulations results in a new earthward propagating fast wave originating from the magnetopause [*Samsonov et al.*, 2007; *Yu and Ridley*, 2011]. We suggest that the successive reflections of the fast shock from the inner boundary and magnetopause studied by *Samsonov et al.* [2007] and oscillations of compressional waves (i.e., cavity mode) in the magnetosphere are the same phenomena. In the MHD theory, the difference between shocks and linear waves concerns only their Mach number. For a fast shock transmitted into the magnetosphere, the fast Mach number is slightly more than unity, and for fast waves it is assumed to be equal to unity. Global MHD codes self-consistently simulate the magnetopause and interaction of any MHD discontinuity or wave with the magnetopause, therefore all transmission and reflection coefficients must be in agreement with the MHD equations.

[12] Summarizing the previous works, we conclude that after a SI passage the dayside region between the ionosphere and the bow shock may contain a mixture of MHD discontinuities and waves (with different periods) propagating transverse to magnetic field, and these waves are able to transform their energy into the field line resonance under some conditions. However, there is a lack of simultaneous observations of the oscillations driven by SI in different magnetospheric regions and in the magnetosheath. Moreover, in this paper we want to inspect the possibility of predicting such oscillations using global MHD codes. We study a magnetospheric SI event observed by several spacecraft near the equatorial plane and compare the observations with results of the global MHD simulation. In section 2, we present solar wind data and overview a 2 h interval of magnetospheric observations. In section 3, we focus on the structure of magnetospheric SI and pay special attention to quasiperiodic ULF pulsations immediately following the SI. We discuss which boundaries may form the oscillating region of compressional waves in agreement with the observed period in section 4. Then we investigate reasons for the appearance of the ULF pulsations in global MHD solutions in section 5. Section 6 contains a discussion of the results and conclusions.

2. Observations and Numerical Results in a 2 h Interval

2.1. Spacecraft Locations and Arrival Times

[13] The IS on 29 July 2002 (day 210) is included in the list of "possible interplanetary shocks" observed by the CELIAS/MTOF Proton Monitor on the SOHO Spacecraft (http://umtof.umd.edu/pm). Its origin is attributed to the M8.7/2N flare on 26 July 21:12 UT and the corresponding full halo CME. The IS was observed by ACE, SOHO, and Wind in the solar wind. In the magnetosphere, the corresponding SI was recorded by Geotail near the dayside magnetopause, by LANL 1990-095 and GOES 8 in the late morning sector, by GOES 10 and Polar in the early morning sector. Note that all the magnetospheric spacecraft were rather close to the equatorial plane. Positions of the spacecraft and the arrival times of IS (in the solar wind) or SI (in the magnetosphere) are summarized in Table 1.

Table 1. Positions of Spacecraft and Times When the Interplanetary Shock and Magnetospheric Sudden Impulse Were Observed

Spacecraft	UT (hh:mm(:ss))	X_{GSM} (R_E)	Y_{GSM} (R_E)	Z_{GSM} (R_E)	MLT[a]
ACE	12:40	243.1	−21.5	36.0	
SOHO	12:43	201.2	51.7	−7.3	
Wind	13:15	26.8	77.7	−28.9	
LANL 1990-095	13:21	5.9	−2.5	−1.6	10.8
Geotail	13:21(:00)	5.7	−8.9	2.4	8.2
GOES 8	13:21(:03)	3.4	−5.7	−0.3	8.1
GOES 10	13:21(:32)	−2.8	−5.7	1.9	4.3
Polar	13:21(:22)	−6.2	−6.7	2.7	3.1

[a]MLT is an estimated magnetic local time for magnetospheric spacecraft.

[14] The IS results in magnetospheric compression observed on the ground by an increase of the SYM-H index (http://wdc.kugi.kyoto-u.ac.jp/aeasy/asy.pdf) at 13:22 UT. Figure 1 shows the SYM-H index and other magnetospheric indices which illustrate the magnetic activity. Immediately after the IS arrival, the magnetosphere is only slightly disturbed, but then the high-latitude currents (such as the Region 1 current) intensify between 14:00 and 14:20 UT as shown by AU and AL plots. At 14:20, a sharp decrease of the SYM-H index results from magnetospheric impact with another solar wind discontinuity discussed briefly below. However our basic attention will be focused on a relatively short interval, about 20 min, immediately after the IS arrival.

2.2. Solar Wind Discontinuities

[15] Figure 2 shows ACE data from 12:00 to 14:00 UT. Temporal profiles obtained from WIND look similar (not shown), but unfortunately WIND plasma parameters have several data gaps. The density at ACE nearly doubles through the IS changing from 6 to 12 cm^{-3} (the WIND density also doubles). The IMF is directed westward and northward, but there is a few seconds dip of negative Bz observed 45 s after the shock front.

[16] We have determined the shock normal using several methods. In method 1, we use a combined approach [*Schwartz*, 2000] collecting information about registration times from SOHO, ACE, WIND and applying the condition $\Delta B_n = 0$ (with ACE magnetic field data). We obtain a shock normal $\mathbf{N}$ = (−0.89; 0.05;0.45) in the GSM coordinates and shock velocity V_{sh} = 484 km/s. In method 2, applying the magnetic coplanarity theorem to the ACE data, we get $\mathbf{N}$ = (−0.85; 0.03; 0.53). In method 3, solving the whole set of the Rankine-Hugoniot equations [*Koval and Szabo*, 2008] with the ACE data, we get $\mathbf{N}$ = (−0.79; −0.24; 0.57) and V_{sh} = 499 km/s. The three methods provide similar results, indicating that the angle between the shock normal and the X axis is about 30–35 degrees and the normal lies nearly in the XZ plane. The difference between the observed jump of SYM-H and our predictions of the IS arrival time obtained from the shock normal and velocity estimations (without taking into account differences of shock speed in the magnetosphere and magnetosheath) does not exceed 2 min using methods 1 and 2, and equal to 7 min using method 3.

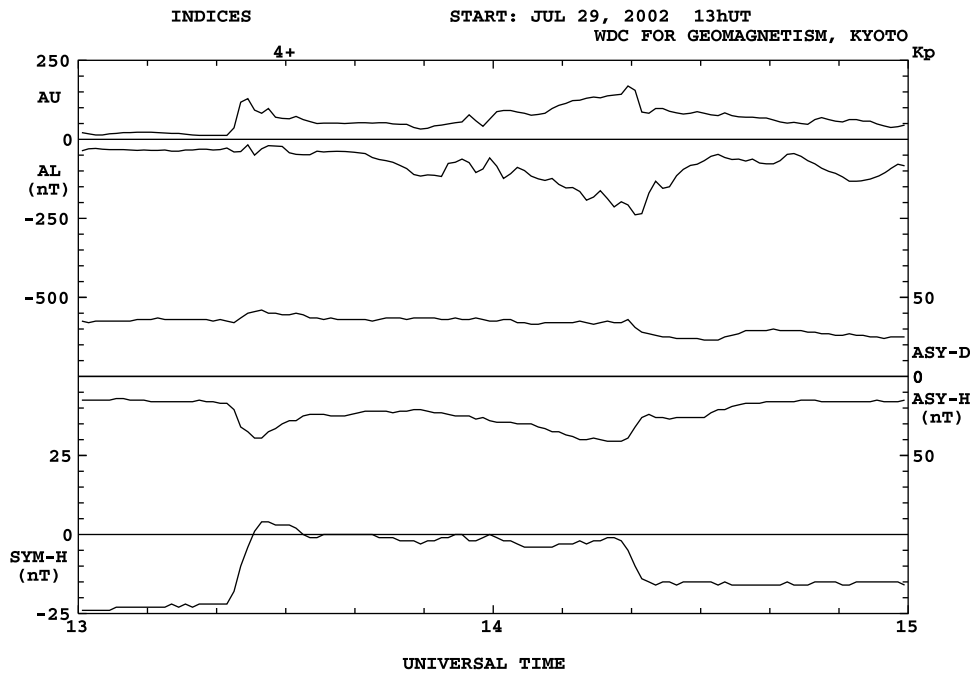

Figure 1. Magnetospheric indices AU, AL, ASYM and SYM-H from the World Data Center for Geomagnetism at the Kyoto University (http://wdc.kugi.kyoto-u.ac.jp).

[17] Using upstream magnetic field and plasma parameters from ACE and the shock normal obtained by method 1, we can estimate the shock's fast mode Mach number

$$M_f = \frac{V_{sh} - \mathbf{V_{up}} \cdot \mathbf{N}}{\sqrt{Vc^2 + Va^2}}$$

where $\mathbf{V_{up}} \cdot \mathbf{N}$ is a scalar product of the upstream flow velocity and shock normal, Vc and Va are the sound and Alfven velocities respectively. The estimation gives $M_f = 2.4$.

[18] About 1 h after the IS, at ~13:34 UT, another discontinuity associated with a change in the IMF direction, a decrease in the proton density, and an increase in the proton temperature passed ACE. The normal of this discontinuity obtained from the Rankine-Hugoniot relations applied to ACE data is (−0.95; −0.31; + 0.11). The ratio $B_n/|B|$ (B_n is the component of the magnetic field along the normal) upstream and downstream from the discontinuity equals 0.026 and 0.032 respectively, and it is found that $|\Delta\mathbf{B}| \simeq |\mathbf{B}|$ (where $\Delta\mathbf{B}$ is the change of magnetic field). These properties resemble a tangential discontinuity (TD). The TD convects with the plasma velocity, its arrival at Earth is determined by a decrease of the SYM-H index at 14:20 UT in agreement with the estimations using the normal orientation. In the interval between the IS and TD (i.e., between first and second SIs), the Earth's magnetosphere was compressed.

2.3. Numerical Models

[19] We have simulated a 2 h interval (corresponding to the solar wind data in Figure 2) using three global magnetospheric MHD codes, i.e., the Block Adaptive Tree Solar wind Roe Upwind Scheme (BATS-R-US) [*Powell et al.*, 1999; *Tóth et al.*, 2005], the Open Geospace General Circulation Model (OpenGGCM) [*Raeder et al.*, 2001], and the Lyon-Fedder-Mobarry global code (LFM) [*Lyon et al.*, 2004; *Merkin and Lyon*, 2010] provided by the Community Coordinated Modeling Center (http://ccmc.gsfc.nasa.gov). We compare the numerical results with magnetospheric observations and find that the numerical predictions from different models are close to each other, but occasionally are significantly different from the observations. Below we give a brief description of the models.

[20] The three global codes solve the single fluid, ideal MHD equations on a three-dimensional grid to simulate the interaction between the solar wind, magnetosphere, and ionosphere. The BATS-R-US and OpenGGCM codes use Cartesian grids, whereas the LFM computational grid is a non-Cartesian, distorted spherical mesh. Spherical grids might be less diffusive in comparison with Cartesian ones in simulations of magnetospheric pulsations because radial and azimuthal oscillations would be better aligned with mesh surfaces. The LFM grid contains 106 × 48 × 64 grid cells. The LFM resolution is 0.16 R_E closest to the SM X-axis, 0.2 R_E about 40 degrees away from the SM X-axis and 0.23 R_E at about 70 degrees away from the SM X-axis (run Andrey_Samsonov_020811_1). The BATS-R-US code uses a block-adaptive Cartesian grid with the finest resolution 0.125 × 0.125 × 0.125 R_E^3 in the whole day side magnetosphere tailward to x = −10 R_E. The OpenGGCM model uses a stretched Cartesian grid with the finest resolution of 0.25 R_E in Y, Z, and 0.125 R_E in X near the magnetopause. Below in this section, we show only results of the LFM and BATS-R-US codes. MHD parameters predicted by the OpenGGCM code vary in a similar way to the shown results.

[21] At the upstream solar wind boundary, we use time-shifted ACE data assuming plane fronts and taking 2 h averaged Vx velocity. The IMF Bx component is fixed and equal to 3 nT during the whole interval. The global models contain no plasmasphere, an average magnetospheric density at the Sun-Earth line is about 0.1, 0.2, and 20 cm^{-3} in the LFM,

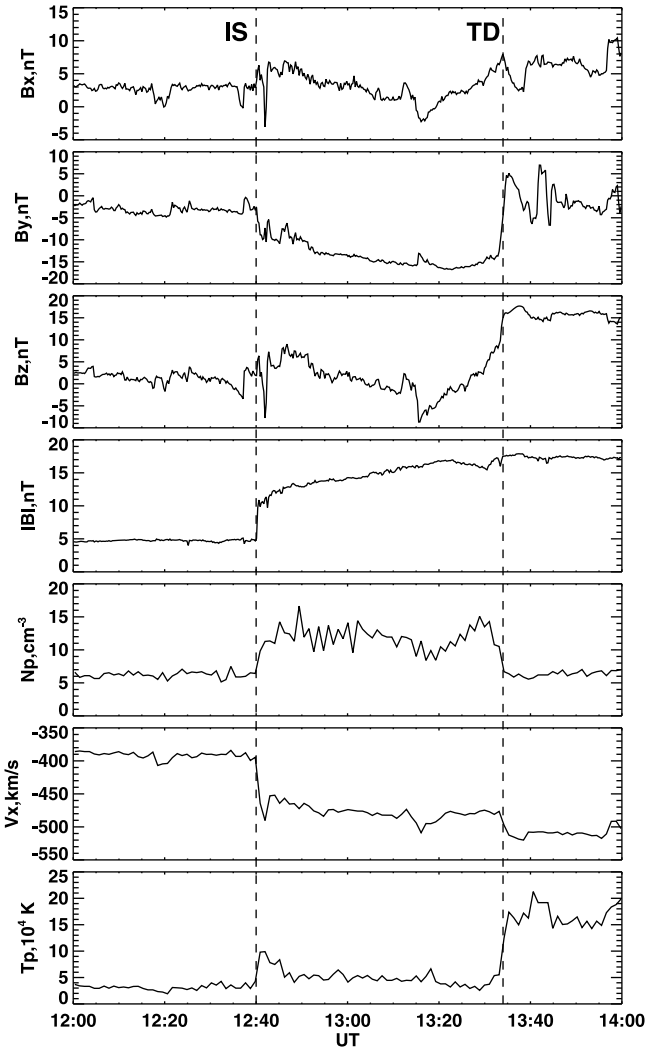

Figure 2. ACE magnetic field and plasma parameters. Two vertical lines mark the arrival of an interplanetary shock and a tangential discontinuity.

OpenGGCM and BATS-R-US models respectively. Such low magnetospheric density in the LFM and OpenGGCM codes results in high Alfven speed which exceeds 10^4 km/s for x < 7 R_E in the subsolar region. The codes use the Boris correction. According to the method described by *Gombosi et al.* [2003], the Alfven speed in areas with strong magnetic field is modified to approach asymptotically to the speed of light and then the speed of light is artificially lowered. The artificial speed of light is 3,000 km/s in the LFM run and 6,000 km/s in the BATS-R-US run. Thus the Alfven speed is kept constant in a significant portion of the dayside magnetosphere in the LFM run, but because of a more dense plasma the Alfven speed in the BATS-R-US run exceeds the limit only near the inner boundary.

[22] The near-Earth boundary of the codes is handled by incorporating a coupled model for the ionospheric electric field. The MHD calculations are stopped near 3 R_E (2.2 for LFM). Field-aligned currents are calculated and mapped along dipole field lines to the ionosphere where they are used as the source term for the height-integrated potential equation. The calculated potential is then mapped back out to the MHD inner boundary where it is used to determine boundary conditions for the velocity and electric field.

2.4. Geotail Data

[23] All magnetospheric spacecraft used in this work observe the SI in a short interval between 13:21 and 13:22 UT (see Table 1). Geotail Editor-B electric and magnetic field measurements with 3 s resolution are shown by black lines in Figure 3, red and blue lines show results of the LFM and BATS-R-US codes along the spacecraft trajectory. Other data from Geotail are not available for this time interval. We will use GSM coordinates throughout the paper, unless another is specified. In Figure 3, the two electric field components are given in GSE coordinates, because we can not convert them to GSM without knowledge of the third component.

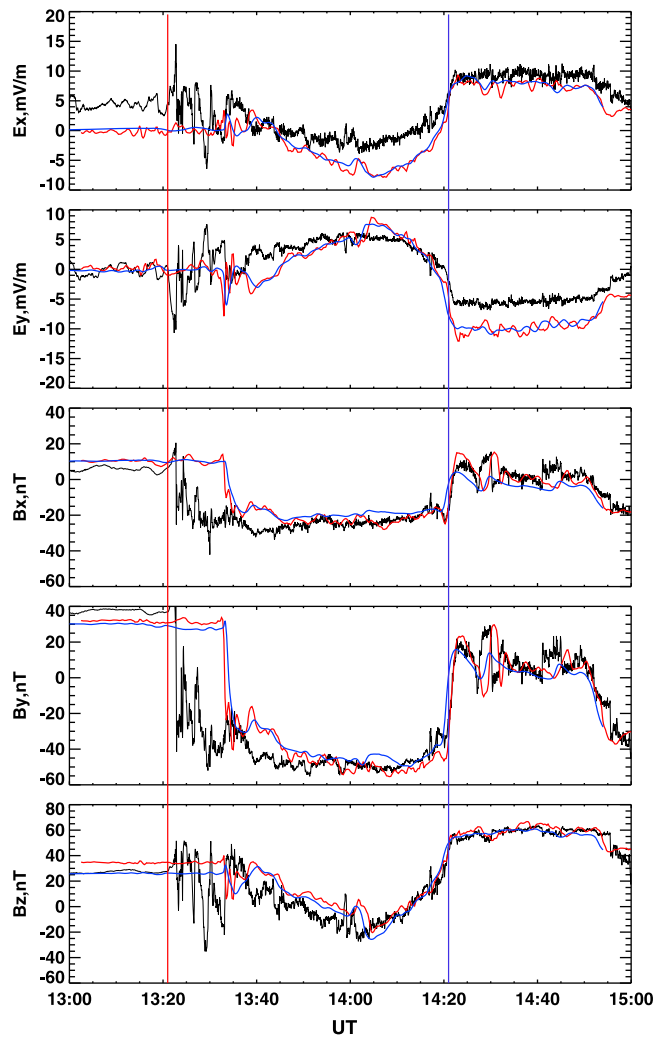

Figure 3. Electric and magnetic field measurements from Geotail (black lines) and simulation results generated by the LFM (red lines) and BATS-R-US (blue lines) global MHD codes. The two electric field components are given in GSE coordinates, whereas the magnetic field components are given in GSM coordinates. Vertical red and blue lines mark the first and second SIs connected with the interplanetary shock and tangential discontinuity respectively.

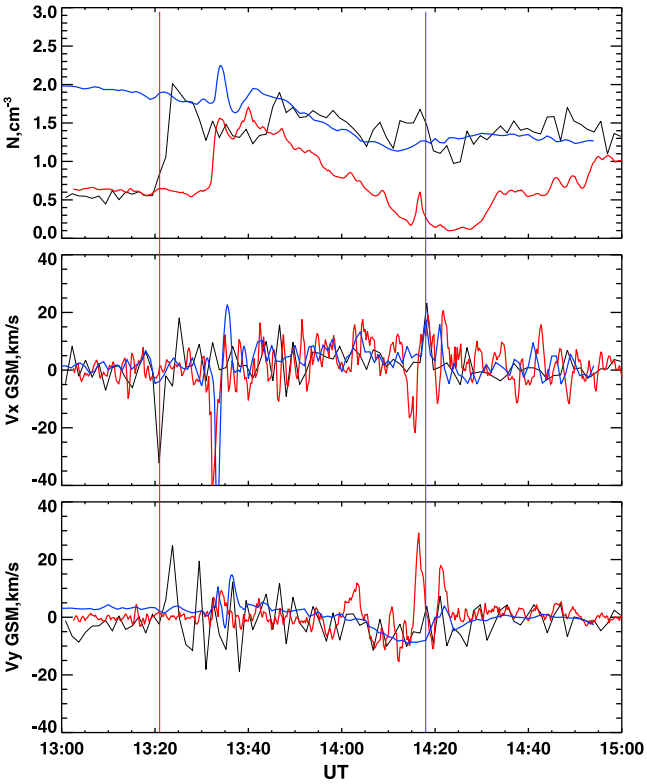

Figure 4. Ion moments measured by LANL 1990-095 (black lines) and predicted by the LFM and BATS-R-US codes (red and blue lines). The LFM predicted density is multiplied by a factor of ten, whereas the BATS-R-US predicted density is divided by a factor of ten.

[24] Geotail registers the SI in the magnetosphere (vertical red line in Figure 3), but about 1 min later the magnetopause moves inward past the spacecraft and Geotail remains in the magnetosheath until the end of the time interval. The second abrupt change of the electric and magnetic field at 14:21 UT corresponds to the arrival of the TD (blue vertical line). The numerical models predict the SI with a ~9 min delay. The delay is explained by the method used for time shifting from the ACE position to the numerical boundary. Time shifting using an average solar wind velocity is not applicable to shocks which move in the plasma flow frame (with a velocity on the order of 100 km/s). On the other hand, the arrival of the second SI at 14:21 UT nearly coincides in the simulations and observations, because the second discontinuity is tangential and propagates exactly with the flow velocity. The MHD simulations predict the inward magnetopause motion almost immediately following the SI in agreement with the crossing observed by Geotail.

[25] Geotail observes intervals both with positive and negative Bz in the magnetosheath, while the IMF Bz is mainly positive with only two intervals of strongly negative values (a short pulse at 12:42 and a more extended interval between 13:15 and 13:25) according to the ACE observations. This difference of the observed magnetic field in the solar wind and magnetosheath probably explains why the simulated Bz before 14:02 UT is slightly higher than the observed one. But in the whole 2 h interval, the agreement between the Geotail observations and simulations in the magnetosheath is reasonably good.

2.5. LANL Data

[26] We have used 86 s resolution ion moments obtained from Magnetospheric plasma analyzer on board of LANL 1990-095. Despite their low resolution, these data provide important information about the ion density and velocity at the dayside geosynchronous orbit. Figure 4 shows the data and numerical results of the LFM and BATS-R-US models along the spacecraft trajectory by black, red and blue lines respectively. The density predicted by the LFM model is one order of magnitude smaller, while the density predicted by the BATS-R-US model is one order of magnitude higher than the observed one, therefore both of them are multiplied by constant coefficients. The amplitude of velocity variations in the 2 h interval predicted by the LFM model is nearly the same as observed one, while the amplitude of velocity variations from BATS-R-US is smaller.

[27] The first SI observed at 13:21 UT (vertical red line in Figure 4) and predicted with an expected delay by the models is distinguished by a threefold density increase and a pulse of negative Vx up to 30 km/s. The negative Vx pulse is followed by a positive Vx pulse of 18 km/s in the LANL data. These features are partly predicted by the numerical models. Both models predict a pulse of negative Vx, but a following pulse of positive Vx is distinctly predicted only by the BATS-R-US, whereas the LFM model predicts irregular oscillations of Vx with amplitude ~10 km/s. At the same time, the LFM model gives qualitatively a better description of the density increase at the first SI. In contrast to the observations, at the second SI the LFM model predicts a pulse of density instead of a density decrease, and a pulse of negative Vx instead of a positive pulse. However, detailed study of the numerical predictions on the impact of solar wind TD is outside the scope of this paper.

2.6. GOES Data

[28] Magnetic field measurements from GOES 8 and GOES 10 with the half-second resolution are shown by black lines in Figures 5 and 6 respectively. Red and blue lines correspond again to the MHD simulations. We take into account the Bz offsets for GOES 8 and 10, equal to 7.22 and 1.04 nT, respectively, found by *Tsyganenko et al.* [2003]. The beginning of the SI is well identified in both GOES 8 and GOES 10 data as abrupt increases in the three magnetic field components, particularly in Bz. The magnetosphere remains compressed until a second SI at 14:19 UT connected with the TD arrival. The solar wind density decreases through the TD, therefore the magnetospheric magnetic field decreases too (i.e., the effect of magnetospheric expansion). The northward IMF component observed by ACE and Wind increases across the TD, correspondingly the dayside magnetospheric magnetic field strength depression caused by Region 1 currents generated during the previous interval of southward IMF weakens and the magnetospheric field grows smoothly after 14:21 UT (14:22 UT in GOES 10 data).

[29] The LFM and BATS-R-US simulations along both the GOES 8 and GOES 10 trajectories predict changes of the magnetic field components quantitatively close to those in data during the first SI. But the models predict the magnetic field observed by GOES 8 better than the field observed by GOES 10 near the second SI. There are systematic differences (on the average about 5–10 nT) between the predicted

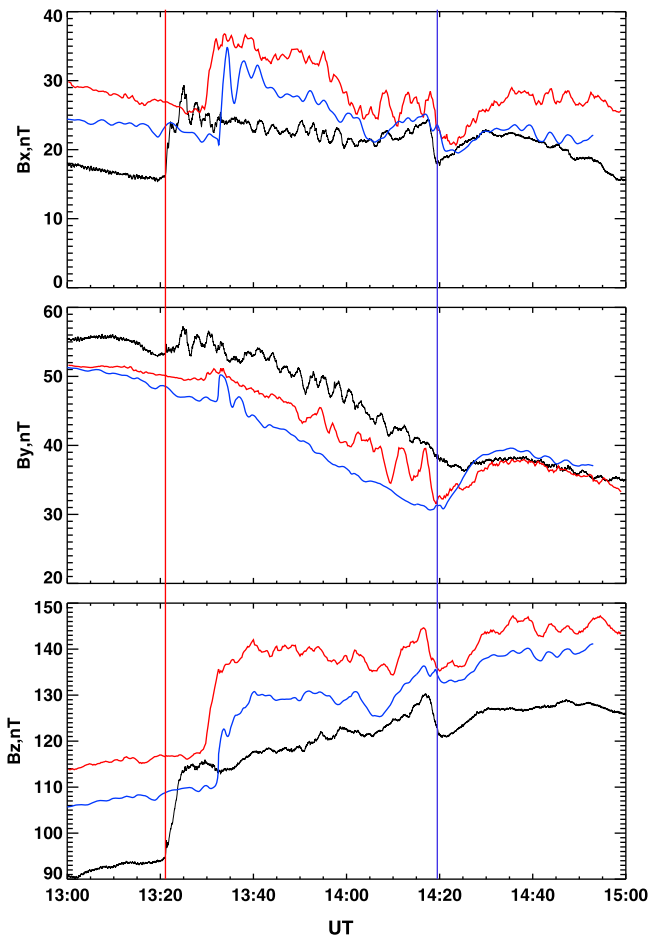

Figure 5. Magnetic field measurements from GOES 8 (black lines) and simulation results from the LFM and BATS-R-US codes (red and blue lines) in GSM coordinates.

and observed values, e.g., the predicted Bz is higher and By is lower than observed during most of the 2 h interval. The discrepancy is also larger for GOES 10 than for GOES 8. It appears that neither model simulates some current systems in the inner magnetosphere very well. Or, it is also possible that the GOES 8 and 10 magnetometers, which are on three-axis stabilized spacecraft, could be in error by several nT since they can only be calibrated once during a spin maneuver at the beginning of spacecraft operations.

2.7. Polar Data

[30] Polar magnetic field observations from the Magnetic Fields Experiment (MFE) and plasma parameters from the Thermal Ion Dynamics Experiment (TIDE) are shown in Figure 7. The resolution of the magnetic field and plasma moments is 6 s. Figure 7 demonstrates large quasiperiodic oscillations of all plasma parameters, including the density and two velocity components throughout the whole interval after the first SI. The oscillations are stronger and more clearly periodic until the second SI at 14:20 UT, i.e., during the interval when the magnetosphere was compressed. The magnetic field variations are more complex and at first glance do not exhibit such clear periodicity as the plasma parameters. The first SI at 13:21 UT causes a smooth ~5 nT increase in the total magnetic field strength over 6 min. Average values of the density and velocity magnitude also increase after the first SI. According to both the numerical MHD modeling results and field line tracing using Tsyganenko's model [*Tsyganenko*, 2002a], Polar remains on closed field lines during this interval.

3. Data Analysis of First Sudden Impulse and Following ULF Waves

3.1. Arrival Times and Internal Structure of Sudden Impulse

[31] The speed with which a sudden impulse propagates through the magnetosphere has been estimated for many events [e.g., *Patel*, 1968; *Sugiura et al.*, 1968; *Wilken et al.*, 1982; *Andréeová et al.*, 2008; *Keika et al.*, 2008]. The estimations are close to the average magnetospheric Alfven velocity of about 1000 km/s which is certainly higher than the velocity of IS in the solar wind for the same events. We make a similar estimation in our case, but should note in advance that such estimations are really not very informative.

[32] First, the Alfven velocity varies between the outer magnetosphere and inner plasmasphere in the range from several hundreds to about two thousand kilometers per second and we can not find the exact spatial distribution of the Alfven velocity from sparse spacecraft observations.

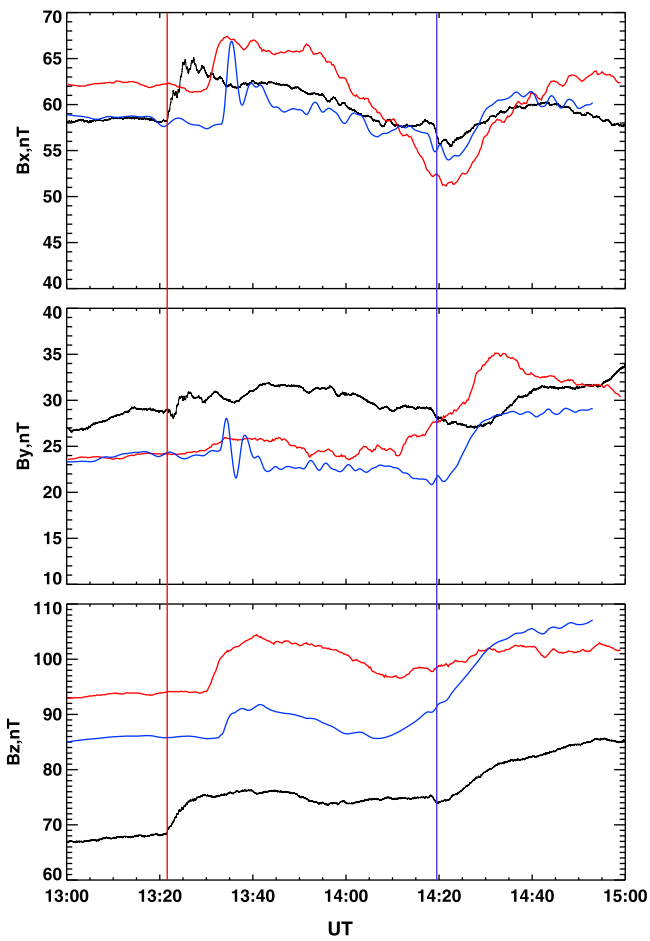

Figure 6. Magnetic field measurements from GOES 10 (black lines) and simulation results from the LFM and BATS-R-US codes (red and blue lines) in GSM coordinates.

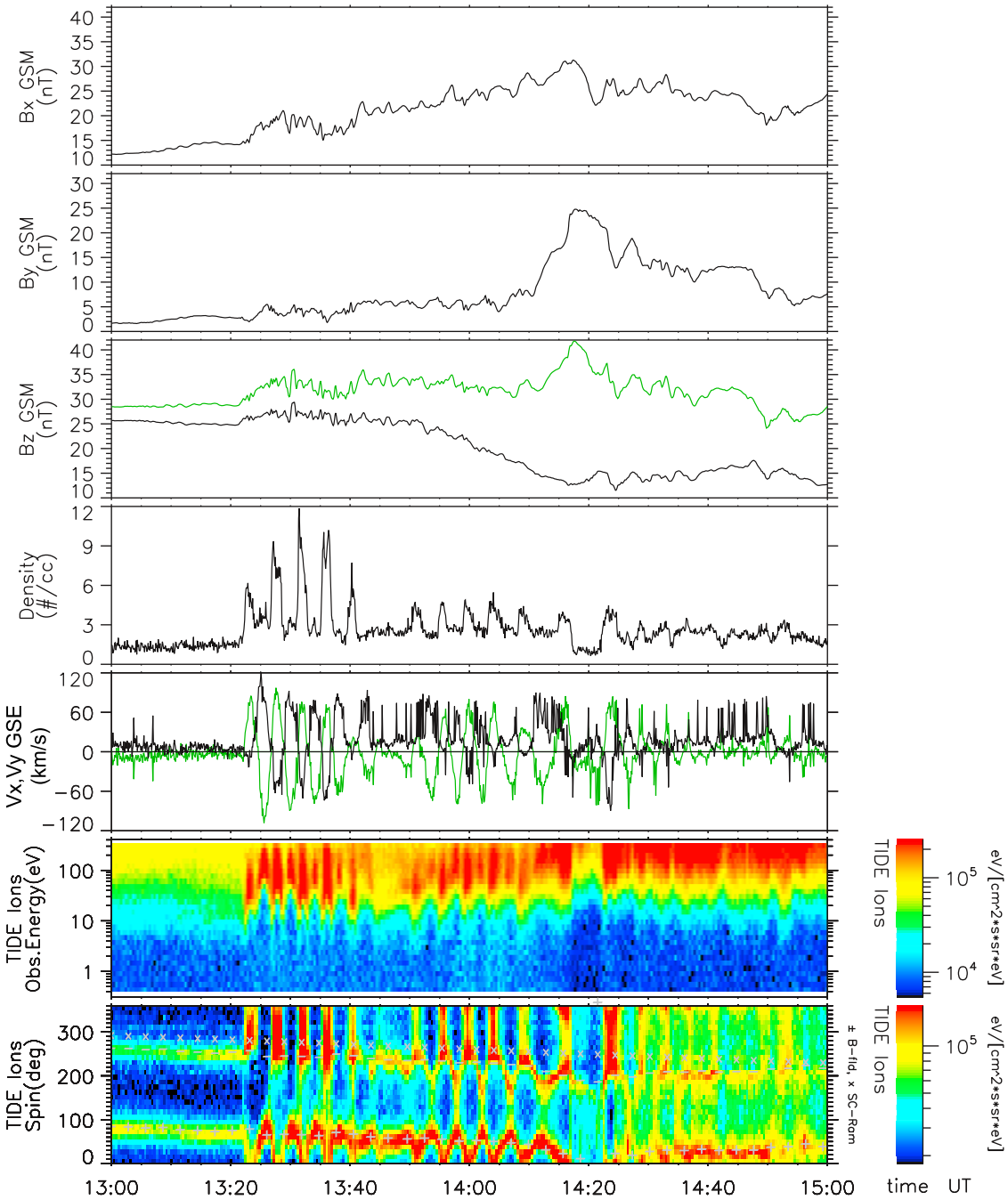

Figure 7. Shown are Polar data: Bx, By, Bz (black) and |*B*| (green) in GSM coordinates, ion density, ion velocity components Vx (black) and Vy (green) in GSE coordinates, spectrograms for ion energy as a function of energy and spin angle.

Moreover, the sudden impulse propagates at the fast mode wave velocity which can differ appreciably from the Alfven velocity in some regions. Thus one can make only a rough estimation of the predicted SI speed.

[33] Second, one needs to get precise arrival times of SI from several spacecraft, but it may be difficult using magnetic field measurements in the magnetosphere. In the supersonic solar wind, the time interval for the magnetic field increase in this event is about 10 s and therefore the shock arrival is unambiguously determined. On the contrary, the corresponding growth of the magnetic field in the magnetospheric SI extends over several minutes at geosynchronous orbit. Figure 8 shows the Bz component from Geotail and the compressional components of the magnetic field (i.e., projection onto the mean vector in the 12-min interval) from GOES 8, GOES 10 and Polar. The high resolution magnetic field measurements reveal that variations of the $B_{||}$ through the SI in some cases differ from a monotonic increase.

[34] GOES 8 registered the SI at geosynchronous orbit near 8 MLT. The SI comprises an initial 16s sharp increase,

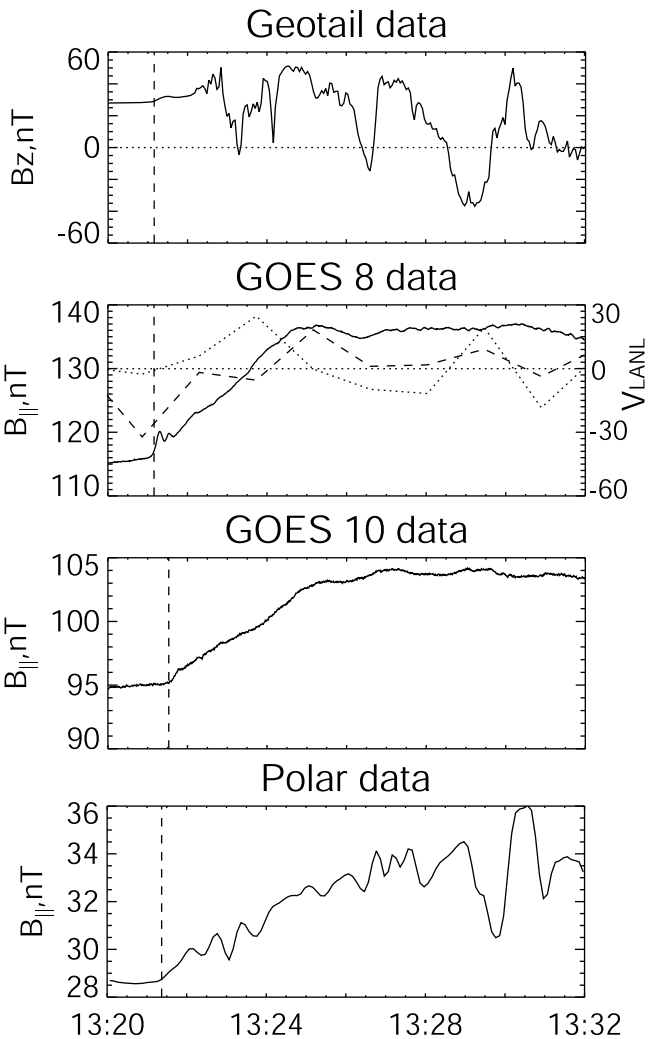

Figure 8. Geotail Bz and compressional magnetic fields observed by GOES 8, GOES 10, and Polar. Additionally, the second panel shows Vx (dashed) and Vy (dotted) LANL 095 ion velocities.

a 30s plateau, and then a 3 min long smooth increase. Such double increases are not unique, e.g., similar variations at the dayside geosynchronous orbit location can be found in Figure 6 of *Andréeová and Přech* [2007] and even more complicated changes observed by GOES 10 are shown in Figure 6 of *Russell et al.* [1999]. The explanation of this structure was given by *Samsonov et al.* [2007]. Using results from a global MHD simulation with the BATS-R-US code, they predict reflection of IS from the inner numerical boundary and connect the first $|B|$ increase with a forward fast shock and the second increase with a reversed/reflected fast shock. In the next several paragraphs, we provide further evidence for this point of view derived from this event.

[35] We superpose variations of the LANL Vx and Vy with variations of the GOES 8 $B_{||}$ in Figure 8. The LANL Vx changes through the SI consist of initial negative (−32 km/s) and subsequent positive (18 km/s) pulses. This can be easily explained by the shock reflection model, because the negative Vx pulse corresponds to the forward fast shock and the positive Vx pulse corresponds to the reversed shock. Although the LANL resolution is low, we find an approximate time between the two extrema equal to ~4.3 min. This is a little longer than the total duration of the SI observed by GOES 8 (~4 min). The reason for the small difference may be connected to the spacecraft positions, because LANL is closer to the Sun-Earth line and this may result in a larger difference between the travel paths of the forward and reversed shocks.

[36] Geotail was very close to the magnetopause at the time when the SI arrived (about one R_E according to simulation results). The jump of Bz through the SI (marked by a vertical dashed line in Figure 8) looks small, because the scale of variations in the magnetosheath is much larger than in the magnetosphere. However the duration of the Bz increase in the Geotail's SI is about 30s, close to the duration of the first step in the GOES 8 data. The variation of the Geotail Bz is 3.8 nT, and the variation of the GOES 8 $B_{||}$ on the first step is 3.6 nT. The total field obtained by the two spacecraft changes by 5.2 and 4.0 nT respectively. Later variations of the Geotail Bz seem to be connected with magnetopause crossings and magnetosheath transients. Therefore we conclude that the variations observed by Geotail and GOES 8 at the beginning of the SI are similar to each other, and the reason for these variations is the forward fast shock coming from the magnetopause. Since Geotail stays in the magnetosheath after ~13:22:10 UT, it cannot observe increases in the magnetospheric magnetic field strength corresponding to the reflected shock, as did GOES 8. However, Geotail observes a consequence of the reflected shock as we show below.

[37] GOES 10 and Polar registered the SI near 3–4 MLT on different L shells. The variations of the GOES 10 $B_{||}$ in the SI are somewhat similar to those at GOES 8. At the beginning of the SI the $B_{||}$ increases by 1.2 nT for 32 s, then a following smooth increase of 7 nT lasts 3.8 min. However, the plateau between the first and second increases is almost absent. This does not contradict the scenario with a reflected shock because this scenario predicts a well-defined two-steps increase only in the dayside magnetosphere (for positive x coordinates).

[38] At a larger L shell (~9.6), Polar observed a more variable $B_{||}$. In the first minute of the SI, $B_{||}$ increases by 1.8 nT, then the average rate of increase becomes lower and the magnetic field fluctuates. The amplitude of magnetic field oscillations in the Polar data increases after the SI.

[39] Finally, we estimate the SI velocity using the GOES 8 and GOES 10 data. As is apparent from above, the arrival time of the forward fast shock (and respectively of the SI) has to be determined at the beginning of the magnetic field strength enhancement (see Table 1). For simplicity, we assume a planar SI front with a normal along the X axis. This gives 1360 km/s which agrees with the average Alfven velocity in the dayside magnetosphere.

3.2. ULF Waves in Geotail and GOES Data

[40] Figure 9 collects magnetic field observations from Geotail, GOES 8 and GOES 10. We choose the one component from each spacecraft which best reflects the periodicity of magnetic oscillations after the SI. The oscillations at geosynchronous orbit are most visible in the azimuthal magnetic field. This is typical for toroidal Alfven waves. At the same time, the periodicity in the Geotail data is better reflected in the Bz component. From 13:22 to 13:34 UT, Geotail observes several transitions from positive to negative Bz which we interpret as a radial magnetopause motion.

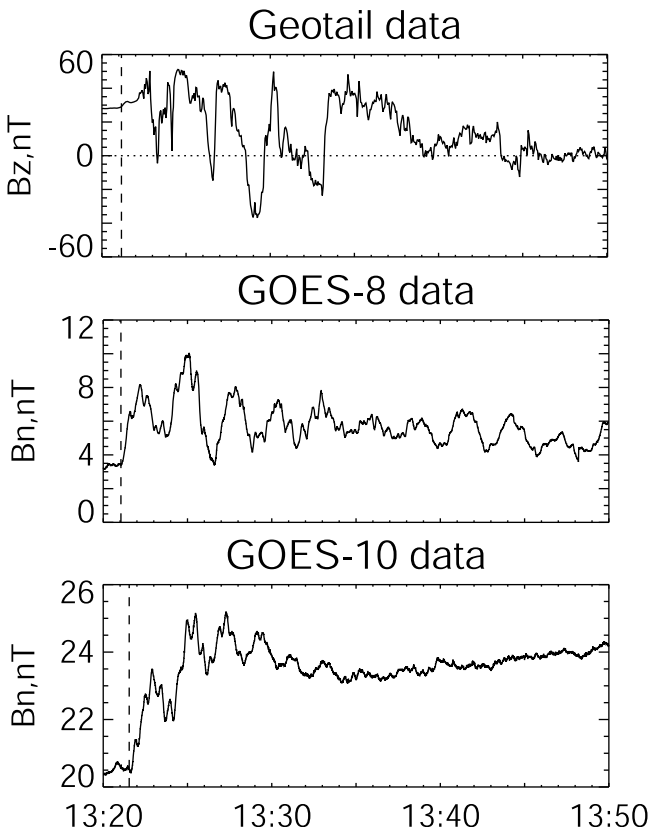

Figure 9. ULF pulsations observed in the Geotail GSE Bz and GOES 8 and GOES 10 azimuthal components Bn after the sudden impulse (vertical dashed line).

[41] As mentioned above, Geotail entered the magnetosheath about 1 min after observing the SI. The magnetosheath magnetic field is usually very disturbed, however we can identify four cycles of roughly quasiperiodical oscillations in Figure 9. Figure 10 shows results from a continuous wavelet analysis (namely the Morlet wavelet with $\omega_0 = 6$) [*Grinsted et al.*, 2004] to better illustrate this periodicity and its time-dependent behavior. The Geotail and GOES 8 data provide evidence for a period of ~3 min between 13:24 and 13:35 UT at the 5% significance level against red noise (within the cone of influence in Figure 10), while the period seen in the GOES 10 data decreases from 2.5 to 2 min and falls below the 5% significance level after 13:30 UT. Note that the oscillation periods in the three panels of Figure 10 are closer to each other at ~13:24 UT, but then behave differently. In Figure 11, we apply a cross wavelet transform to the same Geotail and GOES 8 data and find that both signals vary nearly in-phase.

[42] We can estimate the time required for a compressional wave to traverse the distance between Geotail and GOES 8 moving with a speed of 1000 km/s. Using the positions of the spacecraft in Table 1, we get about half a minute. Since the normal to the compressional wave need not coincide with the vector between the two spacecraft, the travel time may be less. Thus the toroidal wave at geosynchronous orbit seems to be synchronized with the magnetopause oscillations observed by Geotail immediately after the SI. These two types of waves can be connected by a compressional wave which oscillates in the magnetosphere with the same frequency, and GOES 8 really observed such a wave. Figure 12 shows the $|B|$ data from GOES 8 and the corresponding wavelet spectrum. The same 3-min periodicity as shown previously in Figure 10

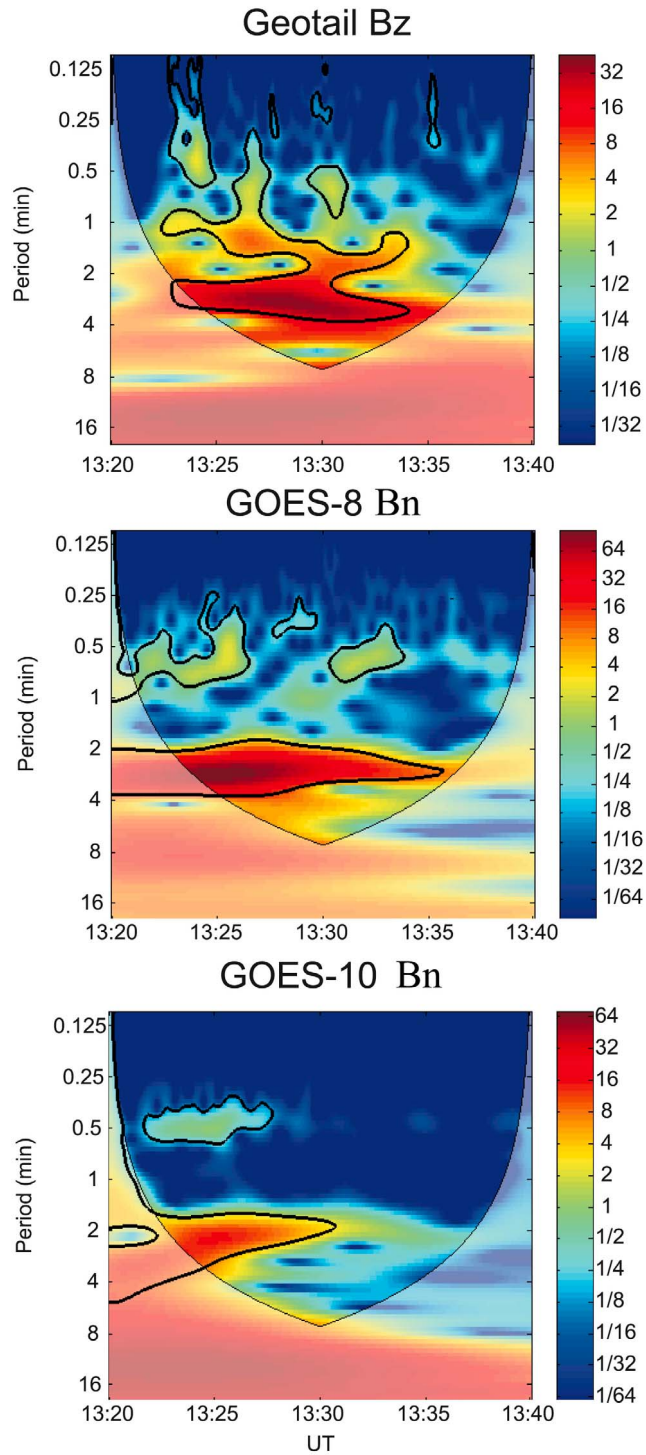

Figure 10. Continuous wavelet power spectra for the magnetic field data shown in Figure 9. The thick contour designates the 5% significance level against red noise. The cone of influence (COI) where edge effects might distort the picture is shown as a lighter shade.

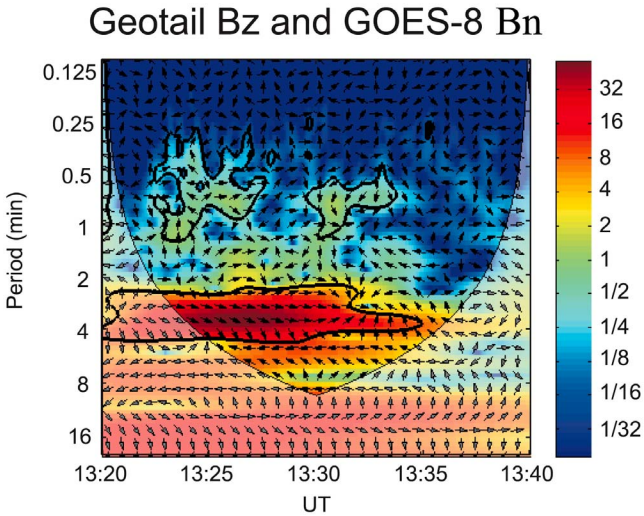

Figure 11. Cross wavelet transform of the Geotail and GOES 8 magnetic field data. The thick contour shows the 5% significance level against red noise. The relative phase relationship is shown as arrows (with in-phase pointing right, antiphase pointing left, and Geotail leading GOES 8 by 90° pointing down).

occurs here too. The periodicity appears immediately after the SI and falls below the 5% significance level after 13:35 UT. Identical results are obtained taking the compressional component $B_{\|}$ instead of the $|B|$.

[43] While the oscillations observed by Geotail and the compressional wave on GOES 8 are quickly damped, the toroidal wave on GOES 8 is visible even after the second SI (e.g., in By in Figure 5). ULF waves with such frequency previously observed at geosynchronous orbit were classified as standing Alfven waves [*Cummings et al.*, 1969].

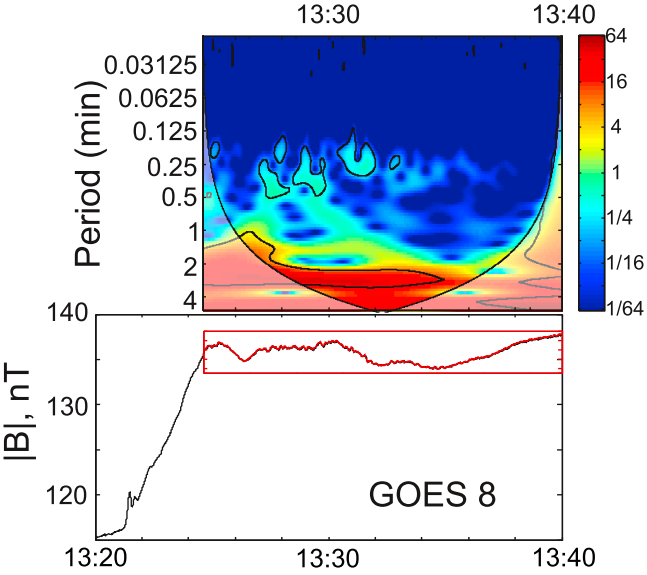

Figure 12. GOES 8 magnetic field magnitude and its wavelet power spectrum in the 15-min interval immediately following the sudden impulse.

3.3. ULF Waves in Polar Data

[44] ULF waves are also prominent in the Polar data shown in Figure 7. The ion density and velocity components strongly oscillate in the 20 min after the SI, then some phase change occurs and slightly weaker irregular oscillations with variable amplitude continue for several hours. Meanwhile, periodicity in the magnetic field data may be not obvious at first glance, therefore we apply the wavelet tool again.

[45] Figures 13a and 13b show continuous wavelet spectrum of the Polar Vx and By data revealing a period of ~4 min in both data sets. Fourier analysis for the interval 13:20–15:00 UT (not shown) also demonstrates this period in the velocity and magnetic field components lying in XY plane. In the interval 13:22–13:40 UT (and later when the periodicity of the magnetic field variations is clear), Vy and By vary nearly in antiphase, therefore these oscillations are not standing Alfven waves.

[46] The density variations observed by Polar may be an artifact, resulting from a cold dense plasma only coming into view when velocities exceed the instrumental energy threshold. Our analysis of the plasma distribution function (not shown) confirms this assumption.

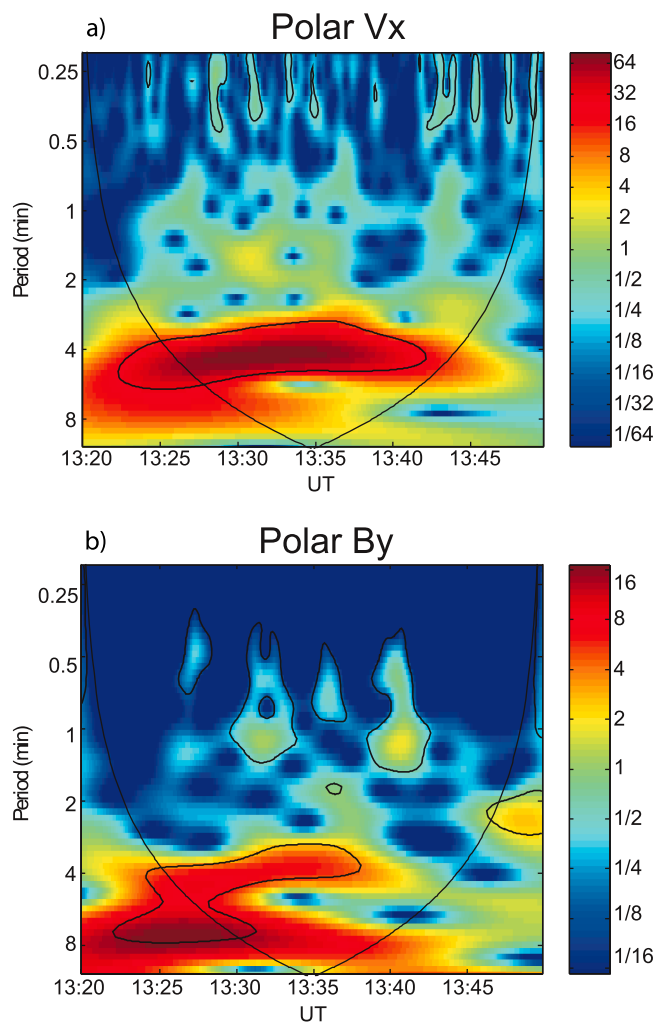

Figure 13. (a) Continuous wavelet power spectrum of Polar Vx. (b) Continuous wavelet power spectrum of Polar By.

Table 2. Approximate Time Intervals When Pulsations Following the Sudden Impulse Were Observed and Their Periods From the Fast Fourier Transform

Spacecraft	Interval	T (min)
Geotail	13:22–13:34	2.6
GOES 8	13:21–14:18	2.6
GOES 10	13:22–13:34	2.3
Polar	13:22–14:18	4.3

[47] Table 2 collects approximate time intervals and mean periods of the observed magnetospheric pulsations from the four spacecraft. The periods have been found using the Fourier analysis (similar values have been obtained from the wavelet power spectra). The SI excites pulsations both in the dayside and nightside magnetosphere, then they gradually attenuate over ~12 min at Geotail and GOES 10, but continue for much longer (at least, until the second SI at 14:18 UT) at GOES 8 and Polar.

4. Boundaries of Oscillating Region

[48] The oscillations with a 2.6-min period were observed after the SI in the Geotail and GOES 8 magnetic field data. This period is dominant in variations of the compressional component $B_{||}$ at GOES 8 and in variations of Geotail *Bz* which we relate to the radial magnetopause motion. We conclude that 3–4 cycles of oscillations of a fast MHD wave occur in the region between inner and outer boundaries. Assuming that the outer boundary is the magnetopause, we estimate the position of the inner boundary using the period obtained from the observations.

[49] For simplicity, the compressional wave is supposed to propagate with the Alfven velocity. We assume a density profile along the Sun-Earth line and the plasmapause position from *Carpenter and Anderson* [1992], and a magnetic field profile from Tsyganenko's model [*Tsyganenko*, 2002a, 2002b]. These profiles and the calculated Alfven velocity profile are shown in Figure 14. Finally, we find the period of a wave oscillating with the Alfven velocity between the magnetopause (placed at L = 11 R_E) and an inner turning point as a function of the position of the turning point. When calculating the magnetic field, we use solar wind parameters before the IS. Were we to take into account the magnetospheric compression after the SI, the period would be even less, because the density profile provided by *Carpenter and Anderson* [1992] depends directly only on the averaged solar activity and not on solar wind conditions. Note that the measured density from LANL 1990-095 (at geosynchronous orbit) varies from 0.5 to 2.0 cm^{-3} through the SI while the predicted value in Figure 14 is 3.9 cm^{-3}. However precise measurements of particles are often difficult outside the plasmasphere, therefore we do not assert a high accuracy for the estimates. Moreover, using the Alfven velocity instead of the fast mode velocity in the estimate may also result in an overestimate of the period.

[50] According to Figure 14, the travel time from the magnetopause to the plasmapause and back is ~80s, which is less than the observed 2.6 min. Placing the turning point at 2 R_E, we get only 130 s which is close, but smaller than the observed period. Since the estimation is rough, we conclude that the oscillations between the magnetopause and the ionosphere would be generally in agreement with the observations.

[51] Using results of global MHD simulations, we can estimate the travel time of a fast MHD wave between the magnetopause and bow shock along the Sun-Earth line. We take profiles calculated by both the LFM and BATS-R-US codes for conditions immediately before the IS arrival and get rather similar results. The total travel time of a fast wave from the magnetopause to the bow shock and back (using the fast mode speed instead of the Alfven speed as above and taking into account the Vx bulk flow velocity in the magnetosheath) equals ~3 min. Correspondingly, the oscillations between the plasmapause and the bow shock may have a period of ~4 min or more. Thus an assumption of such oscillations can hardly explain the observations in this event.

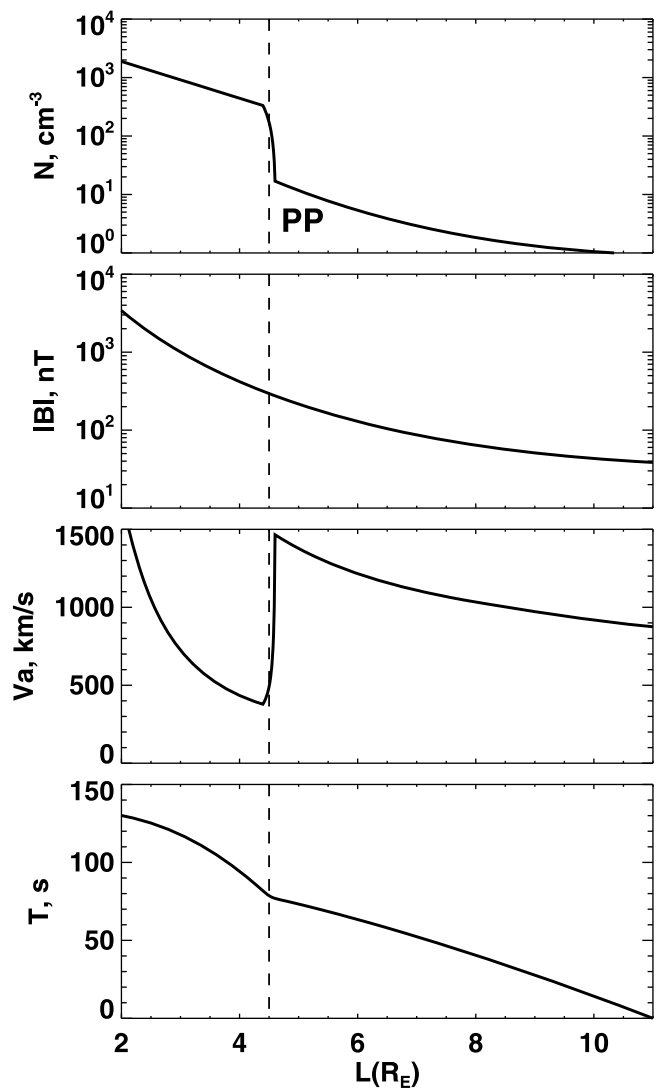

Figure 14. Model density [*Carpenter and Anderson*, 1992] and magnetic field [*Tsyganenko*, 2002a] profiles at the Sun-Earth line and the corresponding Alfven velocity. The last panel shows the period of waves oscillating with the Alfven velocity between the magnetopause (at 11 R_E) and an inner turning point. The vertical dashed line marks the plasmapause.

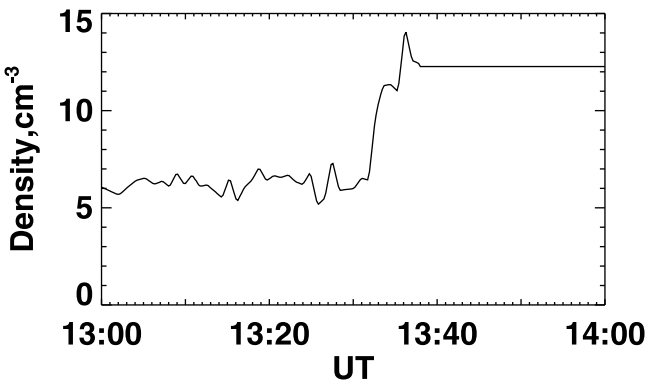

Figure 15. The density at the inflow boundary in a simulation run in which solar wind parameters after the IS were fixed.

[52] The plasmapause is the only distinct boundary between the magnetopause and ionosphere in the dayside magnetosphere, therefore an SI passing through the plasmapause can reach the ionosphere and reflect back. Another possibility is a complete dissipation of the SI during its earthward motion. In this case, toroidal waves observed by GOES 8 and GOES 10 would be excited after only one SI passage. However, this assumption contradicts observations of sunward bow shock motion following the earthward bow shock motion immediately after IS arrival [e.g., *Šafránková et al.*, 2007; *Pallocchia et al.*, 2010]. Moreover, it contradicts observations of the compressional wave following SI in our case and in many previously published papers.

5. Numerical MHD Simulations of ULF Waves After Sudden Impulse

[53] As *Claudepierre et al.* [2010] showed using the LFM global MHD code, strong and continuous solar wind driving results in magnetospheric field lines resonances. In this section, we address the following question: can sudden impulses excite long-lasting ULF waves in MHD models for the magnetosphere. We want to check if one short and strong solar wind impact suffices to generate ULF waves or whether a numerical viscosity in the models causes such waves to dissipate quickly.

[54] Returning to Figures 3–6, one sees some variations in the magnetosphere, for example in the Bx and By components from GOES 8 and GOES 10 predicted both by the LFM and BATS-R-US models. However these variations may simply result from solar wind changes and, hence, they are not magnetospheric resonant waves. We modify the solar wind boundary conditions in order to separate the IS itself from following variations. The solar wind density at the inflow boundary (X = ~30 R_E) for a new run is shown in Figure 15. The density as well as all other input parameters remain fixed after 13:38 UT. We make three runs using the LFM, BATS-R-US and Open GGCM codes with these boundary conditions.

[55] Figure 16 shows results of the numerical simulations and velocity observations from LANL 1990-095. The LANL position is about 3 R_E from the Sun-Earth line. As was mentioned above, both negative and positive Vx pulses are observed by LANL during the SI. The pulses are predicted by all the models, although their magnitude varies from one run to another. LANL observes several oscillations of Vy with amplitude more than 10 km/s after the SI. The simulations qualitatively predict that the amplitude of the velocity oscillations increases immediately after the SI, although the simulated period and amplitude do not match the observed ones.

[56] We have no plasma measurements on board GOES spacecraft, but we present the simulated velocity along the GOES 8 orbit in Figure 17. The negative Vx pulse is clearly distinguished at the SI arrival, but this pulse is followed by several obvious oscillations in the Vx and Vy predicted by all the models. Numerical results along the GOES 10 trajectory (not shown) predict enhanced oscillations after the SI also.

[57] As was shown previously in Figure 7, the plasma moments from Polar strongly oscillate with ~4 min period after the SI. Figure 18 shows the density and two velocity components observed by Polar and the corresponding numerical results. The LFM and OpenGGCM codes clearly reproduce at least the first two cycles of the velocity oscillations. Moreover, the LFM code predicts the following growth of oscillations even when the solar wind conditions are fixed. The periods of predicted and observed oscillations are rather close to each other.

[58] Figure 19 presents a hodogram of the observed and predicted velocities during a 6 min interval. The velocity

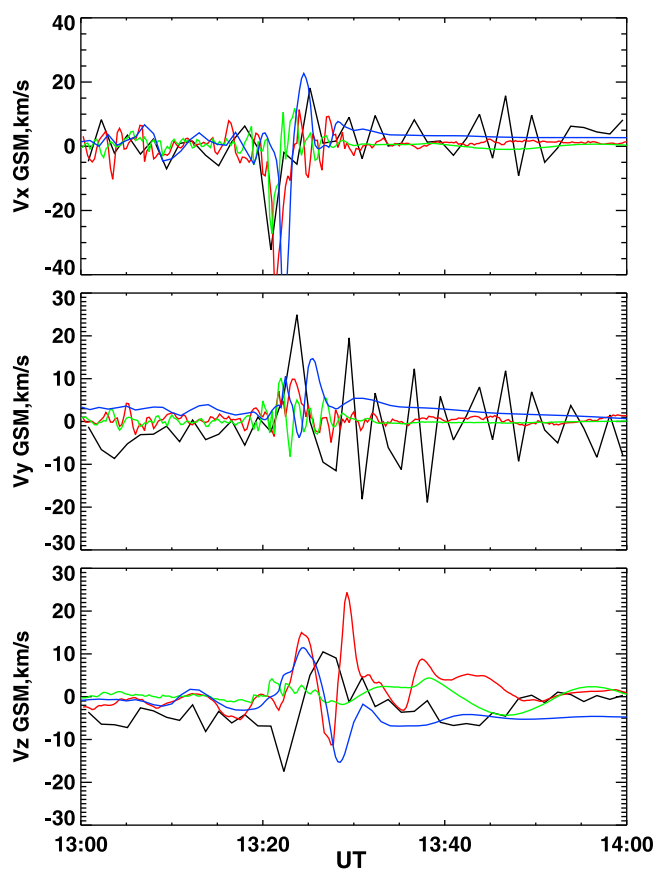

Figure 16. Velocity components observed by LANL (black lines), and predicted by the LFM (red), OpenGGCM (green), and BATS-R-US (blue) global MHD codes. The numerical results are time-shifted for correspondence of SI.

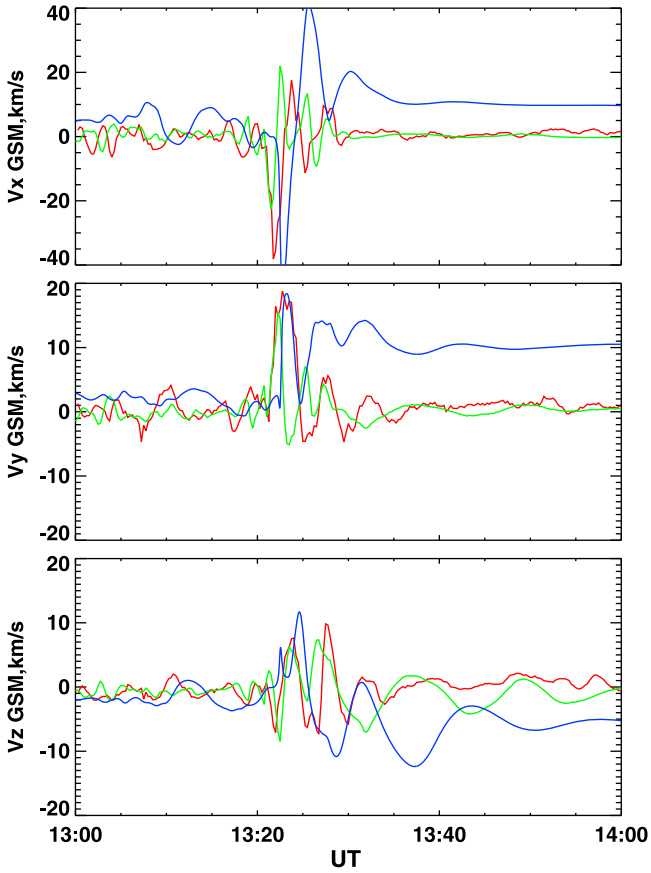

Figure 17. Velocity components predicted by the LFM (red), OpenGGCM (green), and BATS-R-US (blue) global codes along the GOES 8 trajectory.

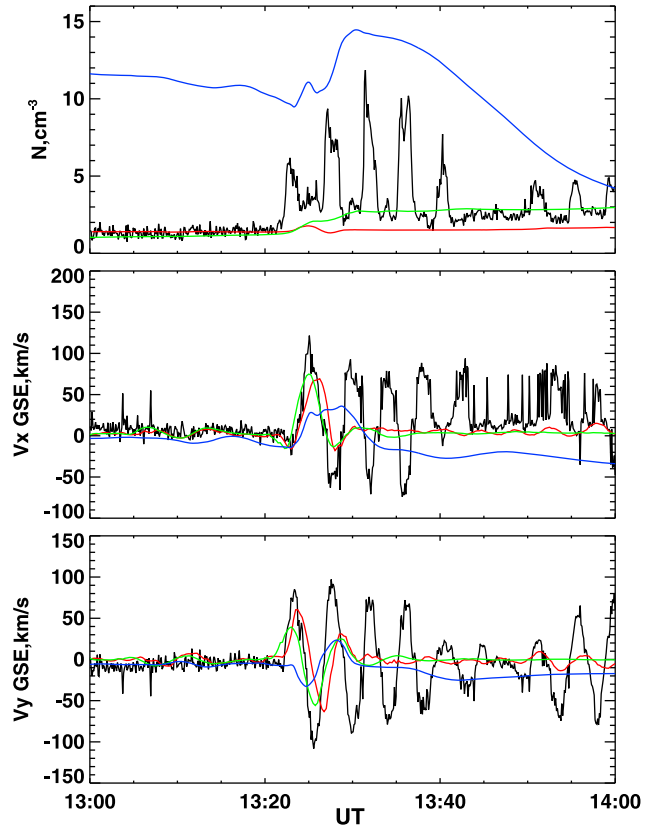

Figure 18. Density and two velocity components observed by Polar (black lines), and predicted by the LFM (red), OpenGGCM (green), and BATS-R-US (blue) global codes. The numerical results are time-shifted, and the simulated density predicted by the LFM and OpenGGCM codes is multiplied by factor 2.

variations lie mainly in the azimuthal direction and have a clockwise rotation both in the data and simulation. Similar oscillations continue later for tens of minutes (as shown in Figure 7).

[59] Now we show how the oscillations predicted along the GOES and Polar trajectories appear in the numerical results of the LFM code. Figure 20 illustrates velocity behavior in the equatorial plane with output frequency every 0.5 min. We select a region which includes positions of GOES 8, GOES 10 and Polar. The magnetopause passes through the region in the bottom right corner. The velocity in the magnetosheath shown by a saturated red color exceeds the upper limit of 200 km/s in the color bar.

[60] A high speed stream in the magnetosphere appears at the right (sunward) boundary at x = 6 R_E in the first panel. The highest magnetospheric velocity is achieved near the magnetopause as shown in the second and following panels (e.g., at (x, y) = (5, −10) R_E in the second panel). In the first two panels the magnetospheric high speed stream is directed nearly tailward, but then earthward and sunward flows become distinctly visible, thus forming a vortex adjacent to the magnetopause. The region where the vortex appears includes the positions of GOES 8, GOES 10, and Polar. The vortex center moves tailward following the IS front. The vortex size extends in the tailward motion and it can disturb the magnetosphere at a distance up to ten Earth radii from the magnetopause (or even more farther tailward).

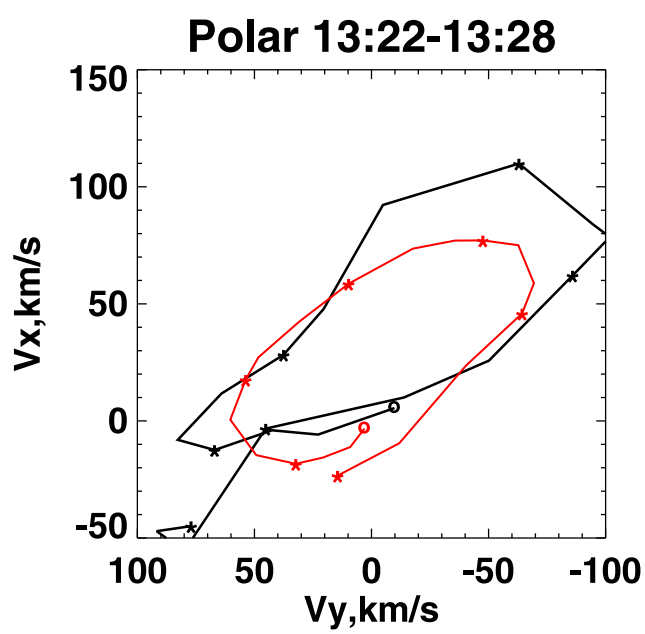

Figure 19. Hodograph of velocity in the XY plane from measurements of Polar (black) and predicted by the LFM code (red). Stars mark every minute, circles show the initial point at 13:22 UT.

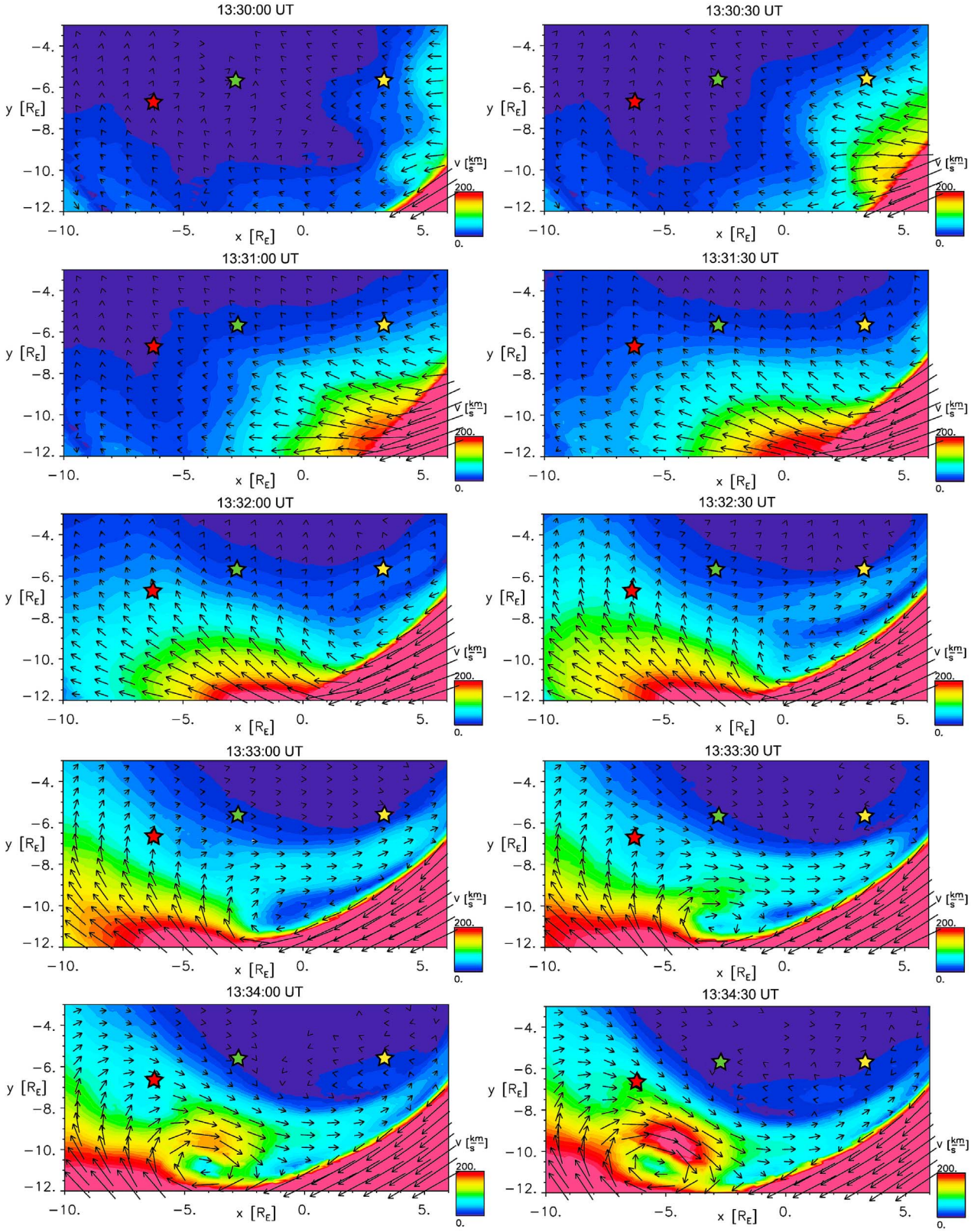

Figure 20. Velocity magnitude and direction predicted by the LFM model in the dawnside magnetosphere in the equatorial plane with output every half minute. Red, yellow and green stars mark positions of Polar, GOES 8, and GOES 10 projected to the equatorial plane.

Inspection of numerical results of the Open GGCM and BATS-R-US codes also reveals formation of vortices in the same region.

[61] Relatively weak magnetic field variations predicted by the LFM code along the Polar trajectory (not shown) oscillate with the same period as the simulated velocity. The LFM model predicts damped velocity oscillations at GOES 8 (see Vy in Figure 17) with the same 4–5 min period; however, as shown above, the period of GOES 8 magnetic field ULF waves is less than 3 min. Thus the simulation can successfully explain only the Polar data.

6. Discussion and Conclusions

[62] This paper presented a comprehensive study of one interplanetary shocks interaction with the magnetosphere on 29 July 2002. Five spacecraft, namely LANL 1990-095, Geotail, GOES 8, GOES 10, and Polar, observed sudden impulses near the equatorial plane in the dawnside magnetosphere at different local times and L-shells. We make numerical simulations of the event using three global MHD models, i.e., the LFM, OpenGGCM and BATS-R-US, and compare the simulations with data.

[63] An interesting feature of the event are ULF waves with periods from 2 to 5 min observed by the above mentioned spacecraft. We interpret the variations of Bz with T = ~2.6 min registered by Geotail at ~8 LT as radial magnetopause oscillations. GOES 8 nearly at the same local time as Geotail observes toroidal and compressional waves with the same period, while GOES 10 at ~4 LT observes waves with T = ~2.3 min. The oscillations at Geotail, GOES 10 and compressional waves at GOES 8 fade away after 3–4 cycles, while the toroidal waves at GOES 8 continue for more than 1 h. We suggest that this may be an example of mode coupling when magnetospheric field line resonances are excited by compressional waves.

[64] LANL 1990-095 measures the plasma moments near the Sun-Earth line. It registers a negative Vx pulse of 30 km/s and a positive pulse of 18 km/s during the sudden impulse. We consider this phenomenon as a direct confirmation of the reflection of fast shock in the inner magnetosphere predicted by *Samsonov et al.* [2007] from results of global MHD simulations.

[65] Generally the interplanetary shock–magnetosphere interaction can be described as follows. An IS propagates through the magnetosheath, interacts with the magnetopause and it results in a fast shock moving earthward through the dayside magnetosphere. Most energy of the fast shock penetrates into the plasmasphere and finally may reach ionospheric heights of several hundreds kilometers where the dayside total ion density rises sharply up to 10^6 cm^{-3}. The fast shock may reflect there and then a reflected fast shock propagates sunward resulting in phenomena like the aforementioned +Vx pulse and the previously studied sunward bow shock motion [e.g., *Šafránková et al.*, 2007]. Compressional waves oscillating in the magnetosphere behave in the same way. We suggest that such waves can oscillate between the magnetopause and the ionosphere, with periods close to those observed. In this paper, we calculate an approximate Alfven velocity profile at the Sun-Earth line using the magnetic field from Tsyganenko's model and the density from *Carpenter and Anderson* [1992]. An estimation of the travel time of a wave moving with the Alfven velocity from the magnetopause to the ionosphere and back gives a value close to the observed periods in our case.

[66] The global MHD codes predict magnetic field increases through the SI and the positive Vx pulse and sunward bow shock motion at the Sun-Earth line related to the reflected shock. But the codes do not predict toroidal and compressional ULF waves like those observed by GOES 8. Since the global codes do not reproduce the plasmasphere, the predicted oscillation period for compressional waves bouncing between the magnetopause and the inner boundary is significantly smaller than those for real waves bouncing between the magnetopause and ionosphere, especially for the LFM and OpenGGCM codes whose magnetospheric densities are less than 1 cm^{-3}. According to our estimation, a fast MHD wave would cross the subsolar magnetosphere from the magnetopause to the inner boundary and back in the LFM run (taking into account the Boris correction) in only 30 s. In principle, such a model cannot reproduce the observed compressional waves with typical periods of several minutes. A similar estimation for the BATS-R-US run gives 110 s, which is close to the observed period. In the last case, we think that the simulations do not predict oscillations near the Sun-Earth line with the given period because of the larger numerical dissipation in the BATS-R-US code. Note also that the MHD codes do not include kinetic effects, like the interaction of Alfven waves with resonant particles, which is supposed to be important for the field line resonance modeling. Although this study does not exclude the possibility that the mode coupling following a solar wind pressure jump can be simulated by MHD codes in the future, the three global codes in our work do not reproduce the observed ULF waves in the dayside magnetosphere for the given event with the given period.

[67] In contrast to the ULF waves observed by Geotail and GOES, Polar observes strong velocity oscillations with a longer period of about 4 min. Using the wavelet tool, we distinguish nearly the same period in By, but not in $|B|$. Vy and By vary nearly in antiphase, therefore these oscillations are not standing waves. A global MHD simulation with the LFM model reproduces velocity variations with the same period. Our study shows that such variations result from large flow vortices originated near the magnetopause. Similar vortices in the global MHD simulations were investigated previously [e.g., *Collado-Vega et al.*, 2007; *Claudepierre et al.*, 2008], but in our case they are created immediately following the IS. Since the solar wind speed increases from 400 to nearly 500 km/s in this event, it is reasonable that the magnetopause flanks become unstable to a high velocity jump. It appears to be the same phenomenon as the Kelvin-Helmholtz instability, but this can be convincingly shown only in a further study. Note that the IMF Bz is mostly positive after the IS according to ACE and Wind data, but it may be negative in the magnetosheath during a 10 min interval from Geotail when the spacecraft observes magnetopause oscillations. The OpenGGCM and BATS-R-US models also predict vortices in the same region.

[68] According to the simulation results, the size of the vortices reaches 10 R_E, therefore they can disturb plasma at geosynchronous orbit. Indeed the predicted velocity components along the GOES 8 trajectory in Figure 17 oscillate

with a similar period as the predicted velocity along the Polar trajectory. However, observed periods of the ULF waves from GOES 8 and GOES 10 are apparently smaller than the 4 min period from Polar. Thus we conclude that the vortices corresponding to the possible Kelvin-Helmholtz instability obtained in the global MHD simulations successfully explain only the Polar observations. A more detailed study of observations at geosynchronous orbit, including plasma data, is needed to understand whether the vortices originated near the magnetopause can make any effect there.

[69] **Acknowledgments.** This work was supported by NASA's Guest Investigator program. A.A.S. thanks Andriy Koval for providing the code for shock normal calculations and Prof. Victor Sergeev for valuable comments. We thank Ruth Skoug for explanations about ACE SWEPAM measurements. This research made use of Geotail data obtained from Data Archives and Transmission System (DARTS), provided by Center for Science-satellite Operation and Data Archives (C-SODA) at ISAS/JAXA. ACE data were provided by the ACE/MAG and ACE/SWEPAM instrument teams at the ACE Science Center (http://www.srl.caltech.edu/ACE/). LANL digital moments were provided by the MPA team through the Coordinated Data Analysis Web (http://cdaweb.gsfc.nasa.gov). Simulation results have been provided by the Community Coordinated Modeling Center (http://ccmc.gsfc.nasa.gov) at Goddard Space Flight Center. The LFM-MIX model was developed at the Center for Integrated Space Weather Modeling (CISM), the OpenGGCM was developed at the University of New Hampshire, and the SWMF was developed at the University of Michigan. We have studied the runs Andrey_Samsonov_082310_2, Andrey_Samsonov_101510_1, Andrey_Samsonov_020811_1, Andrey_Samsonov_021011_1, and Andrey_Samsonov_022211_1.

[70] Robert Lysak thanks the reviewers for their assistance in evaluating this paper.

References

Andréeová, K., and L. Přech (2007), Propagation of interplanetary shocks into the Earth's magnetosphere, *Adv. Space Res.*, *40*, 1871–1880, doi:10.1016/j.asr.2007.04.079.

Andréeová, K., T. I. Pulkkinen, T. V. Laitinen, and L. Přech (2008), Shock propagation in the magnetosphere: Observations and MHD simulations compared, *J. Geophys. Res.*, *113*, A09224, doi:10.1029/2008JA013350.

Araki, T. (1994), A physical model of the geomagnetic sudden commencement, in *Solar Wind Sources of Magnetospheric Ultra-Low-Frequency Waves*, *Geophys. Monogr. Ser.*, vol. 81, edited by M. J. Engebretson, K. Takahashi, and M. Scholer, pp. 183–200, AGU, Washington, D. C.

Baumjohann, W., O. H. Bauer, G. Haerendel, H. Junginger, and E. Amata (1983), Magnetospheric plasma drifts during a sudden impulse, *J. Geophys. Res.*, *88*, 9287–9289, doi:10.1029/JA088iA11p09287.

Baumjohann, W., H. Junginger, G. Haerendel, and O. H. Bauer (1984), Resonant Alfven waves excited by a sudden impulse, *J. Geophys. Res.*, *89*, 2765–2769, doi:10.1029/JA089iA05p02765.

Carpenter, D. L., and R. R. Anderson (1992), An ISEE/Whistler model of equatorial electron density in the magnetosphere, *J. Geophys. Res.*, *97*, 1097–1108, doi:10.1029/91JA01548.

Chen, L., and A. Hasegawa (1974), A theory of long-period magnetic pulsations: 2. Impulse excitation of surface eigenmode, *J. Geophys. Res.*, *79*, 1033–1037, doi:10.1029/JA079i007p01033.

Claudepierre, S. G., S. R. Elkington, and M. Wiltberger (2008), Solar wind driving of magnetospheric ULF waves: Pulsations driven by velocity shear at the magnetopause, *J. Geophys. Res.*, *113*, A05218, doi:10.1029/2007JA012890.

Claudepierre, S. G., M. K. Hudson, W. Lotko, J. G. Lyon, and R. E. Denton (2010), Solar wind driving of magnetospheric ULF waves: Field line resonances driven by dynamic pressure fluctuations, *J. Geophys. Res.*, *115*, A11202, doi:10.1029/2010JA015399.

Collado-Vega, Y. M., R. L. Kessel, X. Shao, and R. A. Boller (2007), MHD flow visualization of magnetopause boundary region vortices observed during high-speed streams, *J. Geophys. Res.*, *112*, A06213, doi:10.1029/2006JA012104.

Cummings, W. D., R. J. O'Sullivan, and P. J. Coleman Jr. (1969), Standing Alfvén waves in the magnetosphere, *J. Geophys. Res.*, *74*, 778–793, doi:10.1029/JA074i003p00778.

Dessler, A. J. (1958), The propagation velocity of world-wide sudden commencements of magnetic storms, *J. Geophys. Res.*, *63*, 405–408, doi:10.1029/JZ063i002p00405.

Dessler, A. J., W. E. Francis, and E. N. Parker (1960), Geomagnetic storm sudden-commencement rise times, *J. Geophys. Res.*, *65*, 2715–2719, doi:10.1029/JZ065i009p02715.

Dryer, M. (1973), Bow shock and its interaction with interplanetary shocks, *Radio Sci.*, *8*, 893–901 doi:10.1029/RS008i011p00893.

Francis, W. E., M. I. Green, and A. J. Dessler (1959), Hydromagnetic propagation of sudden commencements of magnetic storms, *J. Geophys. Res.*, *64*, 1643–1645, doi:10.1029/JZ064i010p01643.

Gombosi, T. I., D. L. De Zeeuw, K. G. Powell, A. J. Ridley, I. V. Sokolov, Q. F. Stout, and G. Tóth (2003), Adaptive mesh refinement for global magnetohydrodynamic simulation, in *Space Plasma Simulation*, edited by J. Büchner, C. T. Dum, and M. Scholer, pp. 247–274, Springer-Verlag, Berlin.

Grib, S. A. (1982), Interaction of non-perpendicular/parallel solar wind shock waves with the Earth's magnetosphere, *Space Sci. Rev.*, *32*, 43–48, doi:10.1007/BF00225175.

Grib, S. A., and E. A. Pushkar (2010), Some features of the interplanetary shock wave interactions connected with the thermal anisotropy and 3D flow past the Earth's bow shock, *Planet. Space Sci.*, *58*, 1850–1856, doi:10.1016/j.pss.2010.08.015.

Grib, S. A., B. E. Briunelli, M. Dryer, and W. Shen (1979), Interaction of interplanetary shock waves with the bow shock-magnetopause system, *J. Geophys. Res.*, *84*, 5907–5921, doi:10.1029/JA084iA10p05907.

Grinsted, A., J. C. Moore, and S. Jevrejeva (2004), Application of the cross wavelet transform and wavelet coherence to geophysical time series, *Nonlinear Processes Geophys.*, *11*, 561–566.

Harrold, B. G., and J. C. Samson (1992), Standing ULF modes of the magnetosphere—A theory, *Geophys. Res. Lett.*, *19*, 1811–1814, doi:10.1029/92GL01802.

Hasegawa, A., K. H. Tsui, and A. S. Assis (1983), A theory of long period magnetic pulsations: 3. Local field line oscillations, *Geophys. Res. Lett.*, *10*, 765–767, doi:10.1029/GL010i008p00765.

Hudson, M., R. Denton, M. Lessard, E. Miftakhova, and R. Anderson (2004), A study of Pc-5 ULF oscillations, *Ann. Geophys.*, *22*, 289–302, doi:10.5194/angeo-22-289-2004.

Keika, K., et al. (2008), Response of the inner magnetosphere and the plasma sheet to a sudden impulse, *J. Geophys. Res.*, *113*, A07S35, doi:10.1029/2007JA012763.

Kivelson, M. G., and D. J. Southwood (1985), Resonant ULF waves: A new interpretation, *Geophys. Res. Lett.*, *12*, 49–52, doi:10.1029/GL012i001p00049.

Kivelson, M. G., J. Etcheto, and J. G. Trotignon (1984), Global compressional oscillations of the terrestrial magnetosphere: The evidence and a model, *J. Geophys. Res.*, *89*, 9851–9856, doi:10.1029/JA089iA11p09851.

Koval, A., and A. Szabo (2008), Modified "Rankine-Hugoniot" shock fitting technique: Simultaneous solution for shock normal and speed, *J. Geophys. Res.*, *113*, A10110, doi:10.1029/2008JA013337.

Lee, D.-H., and M. K. Hudson (2001), Numerical studies on the propagation of sudden impulses in the dipole magnetosphere, *J. Geophys. Res.*, *106*, 8435–8446, doi:10.1029/2000JA000271.

Lee, D.-H., and R. L. Lysak (1989), Magnetospheric ULF wave coupling in the dipole model: The impulsive excitation, *J. Geophys. Res.*, *94*, 17,097–17,103 doi:10.1029/JA094iA12p17097.

Lee, D., and R. L. Lysak (1991), Impulsive excitation of ULF waves in the three-dimensional dipole model: The initial results, *J. Geophys. Res.*, *96*, 3479–3486, doi:10.1029/90JA02349.

Lyon, J. G., J. A. Fedder, and C. M. Mobarry (2004), The Lyon-Fedder-Mobarry (LFM) global MHD magnetospheric simulation code, *J. Atmos. Sol. Terr. Phys.*, *66*, 1333–1350, doi:10.1016/j.jastp.2004.03.020.

Merkin, V. G., and J. G. Lyon (2010), Effects of the low-latitude ionospheric boundary condition on the global magnetosphere, *J. Geophys. Res.*, *115*, A10202, doi:10.1029/2010JA015461.

Pallocchia, G., A. A. Samsonov, M. B. Bavassano Cattaneo, M. F. Marcucci, H. Rème, C. M. Carr, and J. B. Cao (2010), Interplanetary shock transmitted into the Earth's magnetosheath: Cluster and Double Star observations, *Ann. Geophys.*, *28*, 1141–1156, doi:10.5194/angeo-28-1141-2010.

Patel, V. L. (1968), Sudden impulses in the geomagnetotail, *J. Geophys. Res.*, *73*, 3407–3419, doi:10.1029/JA073i011p03407.

Powell, K. G., P. L. Roe, T. J. Linde, T. I. Gombosi, and D. L. de Zeeuw (1999), A solution-adaptive upwind scheme for ideal magnetohydrodynamics, *J. Comput. Phys.*, *154*, 284–309, doi:10.1006/jcph.1999.6299.

Pushkar, E. A., A. A. Barmin, and S. A. Grib (1991), Investigation in the MHD approximation of the incidence of the solar-wind shock wave on the near-Earth bow shock, *Geomagn. Aeron.*, *31*, 522–525.

Raeder, J., et al. (2001), Global simulation of the Geospace Environment Modeling substorm challenge event, *J. Geophys. Res.*, *106*, 381–396, doi:10.1029/2000JA000605.

Russell, C. T., X. W. Zhou, P. J. Chi, H. Kawano, T. E. Moore, W. K. Peterson, J. B. Cladis, and H. J. Singer (1999), Sudden compression of

the outer magnetosphere associated with an ionospheric mass ejection, *Geophys. Res. Lett.*, *26*, 2343–2346, doi:10.1029/1999GL900455.

Šafránková, J., Z. Němeček, L. Přech, A. A. Samsonov, A. Koval, and K. Andréeová (2007), Modification of interplanetary shocks near the bow shock and through the magnetosheath, *J. Geophys. Res.*, *112*, A08212, doi:10.1029/2007JA012503.

Saito, T., and S. Matsushita (1967), Geomagnetic pulsations associated with sudden commencements and sudden impulses, *Planet. Space Sci.*, *15*, 573–587, doi:10.1016/0032-0633(67)90163-8.

Samson, J. C., B. G. Harrold, J. M. Ruohoniemi, R. A. Greenwald, and A. D. M. Walker (1992), Field line resonances associated with MHD waveguides in the magnetosphere, *Geophys. Res. Lett.*, *19*, 441–444, doi:10.1029/92GL00116.

Samsonov, A. A. (2011), Propagation of inclined interplanetary shock through the magnetosheath, *J. Atmos. Sol. Terr. Phys.*, *73*, 30–39, doi:10.1016/j.jastp.2009.10.014.

Samsonov, A. A., Z. Němeček, and J. Šafránková (2006), Numerical MHD modeling of propagation of interplanetary shock through the magnetosheath, *J. Geophys. Res.*, *111*, A08210, doi:10.1029/2005JA011537.

Samsonov, A. A., D. G. Sibeck, and J. Imber (2007), MHD simulation for the interaction of an interplanetary shock with the Earth's magnetosphere, *J. Geophys. Res.*, *112*, A12220, doi:10.1029/2007JA012627.

Samsonov, A. A., D. G. Sibeck, and Y. Yu (2010), Transient changes in magnetospheric-ionospheric currents caused by the passage of an interplanetary shock: Northward interplanetary magnetic field case, *J. Geophys. Res.*, *115*, A05207, doi:10.1029/2009JA014751.

Schwartz, S. (2000), Shock and discontinuity normals, Mach numbers, and related parameters, in *Analysis Methods for Multi-Spacecraft Data*, edited by G. Paschman and P. W. Daly, pp. 249–270, Int. Space Sci. Inst., Bern.

Shinbori, A., T. Ono, M. Iizima, and A. Kumamoto (2004), SC related electric and magnetic field phenomena observed by the Akebono satellite inside the plasmasphere, *Earth Planets Space*, *56*, 269–282.

Southwood, D. J. (1974), Some features of field line resonances in the magnetosphere, *Planet. Space Sci.*, *22*, 483–491, doi:10.1016/0032-0633(74)90078-6.

Sugiura, M., T. L. Skillman, B. G. Ledley, and J. P. Heppner (1968), Propagation of the Sudden Commencement of July 8, 1966, to the Magnetotail, *J. Geophys. Res.*, *73*, 6699–6709, doi:10.1029/JA073i021p06699.

Tamao, T. (1964), The structure of three-dimensional hydromagnetic waves in a uniform cold plasma, *J. Geomagn. Geoelectr.*, *16*, 89–114.

Tóth, G., et al. (2005), Space Weather Modeling Framework: A new tool for the space science community, *J. Geophys. Res.*, *110*, A12226, doi:10.1029/2005JA011126.

Tsyganenko, N. A. (2002a), A model of the near magnetosphere with a dawn-dusk asymmetry: 1. Mathematical structure, *J. Geophys. Res.*, *107*(A8), 1179, doi:10.1029/2001JA000219.

Tsyganenko, N. A. (2002b), A model of the near magnetosphere with a dawn-dusk asymmetry: 2. Parameterization and fitting to observations, *J. Geophys. Res.*, *107*(A10), 1176, doi:10.1029/2001JA000220.

Tsyganenko, N. A., H. J. Singer, and J. C. Kasper (2003), Storm-time distortion of the inner magnetosphere: How severe can it get?, *J. Geophys. Res.*, *108*(A5), 1209, doi:10.1029/2002JA009808.

Walker, A. D. M., J. M. Ruohoniemi, K. B. Baker, R. A. Greenwald, and J. C. Samson (1992), Spatial and temporal behavior of ULF pulsations observed by the Goose Bay HF radar, *J. Geophys. Res.*, *97*, 12,187–12,202, doi:10.1029/92JA00329.

Wilken, B., C. K. Goertz, D. N. Baker, P. R. Higbie, and T. A. Fritz (1982), The SSC on July 29, 1977 and its propagation within the magnetosphere, *J. Geophys. Res.*, *87*, 5901–5910, doi:10.1029/JA087iA08p05901.

Wilson, C. R., and M. Sugiura (1961), Hydromagnetic interpretation of sudden commencements of magnetic storms, *J. Geophys. Res.*, *66*, 4097–4111, doi:10.1029/JZ066i012p04097.

Yu, Y.-Q., and A. J. Ridley (2011), Understanding the response of the ionosphere-magnetosphere system to sudden solar wind density increases, *J. Geophys. Res.*, *116*, A04210, doi:10.1029/2010JA015871.

Zhou, X., and B. T. Tsurutani (2001), Interplanetary shock triggering of nightside geomagnetic activity: Substorms, pseudobreakups, and quiescent events, *J. Geophys. Res.*, *106*, 18,957–18,968, doi:10.1029/2000JA003028.

W. Baumjohann, H. K. Biernat, and A. A. Samsonov, Space Research Institute, Schmiedlstrasse 6, A-8042 Graz, Austria. (baumjohann@oeaw.ac.at; helfried.biernat@oeaw.ac.at; andre.samsonov@gmail.com)

S.-H. Chen, NASA Goddard Space Flight Center, Mail Code 673, 8800 Greenbelt Rd., Greenbelt, MD 20771, USA. (sheng-hsien.chen@nasa.gov)

L. Rastaetter and D. G. Sibeck, NASA Goddard Space Flight Center, Mail Code 674, 8800 Greenbelt Rd., Greenbelt, MD 20771, USA. (lutz.rastaetter-1@nasa.gov; david.g.sibeck@nasa.gov)

H. J. Singer, Space Weather Prediction Center, 325 Broadway, Boulder, CO 80305, USA. (howard.singer@noaa.gov)

N. V. Zolotova, Department of Earth Physics, Saint Petersburg State University, Ulyanovskaya 1, Petrodvorets, St. Petersburg, 198504, Russia. (ned@geo.phys.spbu.ru)